GSA DATA REPOSITORY 2018209

Supplementary text, figures and tables to
"Rapid formation of porphyry copper deposits evidenced by diffusion of oxygen and titanium in quartz"
F. Cernuschi, J. H. Dilles, S. B. Grocke, J. W. Valley, K. Kitajima, and F. J. Tepley III

INDEX

Porphyry Cu±Mo±Au Deposits

Porphyry copper deposits include porphyry Cu±Mo±Au deposits in which copper is the chief economic metal. These deposits are large, ranging from <0.1 Mt (megatonnes) to >90 Mt contained copper, with ore grades ranging from <0.2 to >1.2 wt.% Cu with variable amounts of Mo and Au. The largest single deposit, albeit formed in multiple temporally spaced hydrothermal events introduced over several million years, is the El Teniente deposit, Chile (~96 Mt contained Cu), and perhaps the largest single hydrothermal event (<100,000 years; von Quadt *et al.,* 2011) is the Bingham, Utah, Cu-Au orebody (~28 Mt contained Cu). Porphyry copper deposits can be subdivided according to the tonnage of contained copper: <0.1 Mt Cu (small); 0.1 to 0.3162 Mt Cu (moderate); 0.3162 to 1.0 Mt Cu (large); 1.0 to 3.162 Mt Cu (very large); 3.162 to 10 Mt Cu (giant); 10 to 31.62 Mt Cu (supergiant); >31.62 Mt Cu (behemoths; Clark, 1993 and Cooke and Hollings, 2005).

In well-exposed porphyry deposits, a deep source intrusion, commonly estimated at >50 km^3 but as much as 500 km^3 (Ruby Star Granodiorite: Stavast *et al.,* 2008; El Abra Fiesta Granodiorite; Brimhall *et al.,* 2006; Dilles *et al.,* 2011) that is an equigranular granitoid is commonly exposed (see Burnham, 1979). These intrusions range from quartz diorite to granite to monzonite, and span the range from Na-rich to K-rich calc-alkaline to alkaline. Most intrusions are metaluminous, but some are weakly peraluminous or near the boundary of metaluminous to peralkaline (Seedorff *et al.,* 2005). The deep granitoid is the source of porphyry dikes of identical composition but with a porphyritic texture characterized by ~50 vol.% fine-grained groundmass that is commonly <0.1 mm in grain size, granitic in composition, and aplitic in texture. Such aplite represents a pressure-quench via water-vapor loss on ascent of magma at relatively low temperature (~700°C) (Burnham, 1979; Dilles, 1987). At Yerington and several porphyry deposits in the southwest of the USA, such porphyry dikes can be observed to grade downward into the deep granite, and moreover that younger dikes are more deeply sourced and cross-cut older dikes with slightly coarser groundmass (Dilles, 1987).

The formation of large and giant porphyry copper deposits requires the release of a large mass of magmatic-hydrothermal fluid from the source intrusion. This can be estimated by calculating the mass required to form the amount of quartz added in veins by hydrothermal fluids. To form the quartz veins observed in the Ann-Mason deposit in the Yerington district, 11 Mt of silica had to be transported by the hydrothermal fluid. This requires the release of 2.6 Gt of magmatic water from the Luhr Hill granite (Anne Schopa and John Dilles personal communication and Schopa *et al.,* 2017). According to Dilles (1987), the Luhr Hill granite volume can be estimated in 80 km^3 of magma or 200 Gt. The water content of the granite is ~ 4 wt. %, therefore, the granite hosted ~ 8 Gt of magmatic fluid. The amount of Cu lost from the 200 Gt Luhr Hill granite was estimated in 50 ppm, therefore, the 8 Gt of released fluid could have form up to 10 Mt of Cu. This estimate suggests that the released fluids from the granite may have formed the ~ 8 Mt PCD ore hosted in the district. In summary, at least 2Gt of fluid are required to form ~4Mt of Cu-ore.

As reviewed by Seedorff *et al.* (2005), porphyry deposits may form at a variety of depths in the upper crust ranging from as shallow as ~1 km for copper mineralization

(*e.g.*, Batu Hijau, Yerington Mine) to ~10 km (*e.g.*, Butte, Montana; 6-8 km). Shallow deposits are characterized by "A" type granular quartz-sulfide veins, whereas deep deposits lack these veins but instead contain early dark micaceous (EDM) veins as at Butte (Proffett, 2009). Shallower deposits likely form at slightly lower temperature and presumably may cool more quickly after fluid flow ceases. The range of observed hydrothermal temperatures in such deposits ranges from ~700°C at Butte (Brimhall, 1977; Field *et al.,* 2005; Rusk *et al.,* 2006; Mercer *et al.,* 2013) to about 300°C for late base metal veins associated with strong sericitic alteration (*e.g.* Rusk *et al.,* 2008; Landtwing *et al.,* 2005). Oxygen and hydrogen isotopic data suggest that all hydrothermal fluids that produce K-silicate and sericitic alteration are magmatic in origin at temperatures of 700 to 350°C (Harris and Golding, 2002; Zhang, 1995), consistent with thermal models of fluid flow (Weis *et al.,* 2012).

The Haquira East Porphyry Copper Deposit

The Haquira district contains two known porphyry copper centers. Haquira East is the focus of this study (-14.164877º, -72.345922º), and is the subject of the PhD thesis of Cernuschi (2015). Haquira East is a relatively large porphyry copper deposit with minor Mo and Au that contains measured, indicated, and inferred resources of 689 Mt ore containing 4.2 Mt Cu (~9 B lb), about 37,000 t Mo, and 28 t (0.9 M oz) Au (Antares, 2010). Haquira East is a relatively typical, but also a relatively deeply formed, porphyry copper deposit. A variety of evidence suggests Haquira formed at relatively great depth for a porphyry deposit. "A" type quartz veins are rare, and EDM veins are the largest contributors to Cu grades (Proffett, 2009; Cernuschi *et al.,* 2012). Late, low-temperature ~350 °C D pyrite-quartz veins with sericitic selvages and late <300 ºC pyrite veins with intermediate argillic alteration are rare (affecting <5% of the granodiorite porphyry stock). All observed fluid inclusions contain liquid and a moderate-sized vapor bubble, and were therefore trapped in quartz veins that formed at pressures greater than those that lead to fluid immiscibility (*i.e.* in the single-phase field); there are no observations of brine or vapor-rich inclusions indication fluid immiscibility. These inclusions were therefore trapped at >1.4 kb pressure. Fluid inclusion heating / freezing experiments provide homogenization temperatures and bulk salinities, which may be used together with appropriate P-T isochores, and comparison with Ti-in-quartz and phase petrology temperature estimates to estimate trapping pressures of between 1.6 kb and 3 kb at near-lithostatic pressures (Cernuschi, 2015). The fluid inclusion population more closely resembles the population at Butte, Montana where liquid plus vapor fluid inclusions dominate. However, at Butte fluid inclusions with trapped brines and vapors are rarely observed, and indicate that some fluid un-mixing occurred. Therefore, it is likely that Haquira East was emplaced at a greater depth than Butte where Rusk *et al.* (2008) estimated pressures of 2.0 to 2.5 kb for high temperature veins and a depth of emplacement of ~8 km.

Hydrostatic conditions must have prevailed at low temperatures below ca. 300-400°C in a zone that initially was above the Haquira East porphyry deposit but extended into the ore zones during formation of the late stage sericitic alteration and even later intermediate argillic alteration.

Moreover, geologic considerations also indicate great depth. Hornblende barometry of the nearby exposed and shallower Acojasa granodiorite pluton yields a pressure estimate of ~ 2 (±0.5) kb (Cernuschi, 2015, and references therein). The Acojasa and other associated intrusions are inferred to be concealed at depth below the meta-sedimentary succession that is preserved at Haquira East and are likely the source of the granodioritic stock, dikes and magmatic-hydrothermal fluids. One-kilometer deep drill-holes did not reach the top of the inferred source intrusion below it. Therefore, the lithostatic pressure during the emplacement of Haquira East could have been > 2 kb. Furthermore, hornblende barometry of other intrusions in the Andahuyalas batholith at the Coroccohuayco Cu-skarn/porphyry deposit (Tintaya cluster) also yield high pressure, ranging from 1.4 to 2.4 Kbar (Chelle–Michou, 2013).

Nonetheless for purposes of this manuscript, we use conservative estimates of ~1.4 kb lithostatic pressure for high temperature hydrothermal conditions that transition to close to hydrostatic pressures at ~1.1 kb. Quartz phenocrysts (except the bright-CL rims) formed in an underlying magma chamber, so they likely formed at 2-3 kb pressure.

The Haquira East deposit is hosted in a granodiorite porphyry plug that intrudes a folded and ductile deformed quartzite sequence. Hydrothermal banded molybdenite-quartz (BMQ) veins cutting the quartzite are locally folded, and hydrothermal biotite in the porphyry plug is aligned into a foliation by deformation. This deformation does not affect the last porphyry dikes, which has an isotopic age that is indistinguishable from the earlier porphyries. Therefore, deformation was ongoing during porphyry emplacement, and suggests significant depth and >350°C for the rocks surrounding the deposit. As muscovite has a closure temperature to Ar diffusion of ~325-350°C (depending on grain size), the $^{40}Ar/^{39}Ar$ age of muscovite likely reflects slow cooling after the end of hydrothermal alteration. Hence, the hydrothermal lifespan is likely shorter than the 200,000 to 600,000 year interval defined by the Re-Os age of molybdenite and the $^{40}Ar/^{39}Ar$ age of muscovite. Average of 3 molybdenite ages is 33.75 ± 0.15 Ma and one $^{40}Ar/^{39}Ar$ age of muscovite yields 33.18 ± 0.21 Ma (Cernuschi *et al.,* 2013).

Extended Methods

Secondary Electron Microscope Cathodoluminescence (SEM-CL)

SEM-CL images of 30 and 200 μm thick polished sections were obtained at the Oregon State University Microscopy facility using a FEI Quanta 600FEG with a Gatan mini-CL detector with a wavelength range between 185 and 850 nm. Images were obtained while operating the instrument between 10 and 15 KeV, a spot size of 6 μm, scanning time between 50 and 200 μs and resolution of 1024x884 pixels. Thin sections were carbon coated or gold coated (< 100 nm thick) prior to the analyses. Gray scale profiles were obtained using NIH ImageJ software. For each profile the gray line shows the raw gray scale data and the black line represents a smoothed profile calculated by ImageJ. The smoothed profile is calculated by averaging contiguous pixel scale CL-intensity variations and is considered a better representation of the gray scale variations at the micron scale.

Electron Microprobe (EMP)

Titanium and aluminum in quartz on the thin section samples previously imaged by SEM-CL were obtained at Oregon State University using a CAMECA SX-100 Electron microprobe (EMP), by simultaneously collecting Ti x-rays on one LPET and two PET diffracting crystals, and collecting Al x-rays on one TAP and one LTAP diffracting crystals, a 15 keV accelerating voltage, a 200 nA beam current, a 1 um spot diameter and 600 second counting times on peak and 300 seconds on each background peak. Ti and Al detection limits of 13 ppm are calculated using three standard deviations of the counting rate for the background (3 sigma). With multiple diffraction crystals, this is the equivalent of 1800 seconds on peak and 900 seconds on each background peak for Ti, and 1200 seconds on peak and 600 seconds on each background peak for Al. We used rutile and as the primary standards for Ti and Al, and analyzed a Shandong quartz as a secondary standard (Shandong, Audétat *et al.,* 2014) routinely for Ti and Al concentrations between analyzes of unknown samples (Table A1). We obtained 58 ± 6 ppm Ti and 133 ± 7 ppm Al for 18 analyses of Shandong, which is comparable to the 57 ± 4 Ti ppm and 154 ± 15 ppm Al reported by Audetat *et al.* (2015).

Laser Ablation Inductively Coupled Plasma Mass Spectroscopy (LA-ICP-MS)

The LA-ICP-MS analyses at Oregon State University were obtained by using a Photon Machines Analyte G2 laser operating at 7 Hz with a 85 μm fixed spot and drilled to ~ 20 μm depth (Loewen and Kent, 2012; Dumitru et al., 2013). The total number of laser shot was 225 per analysis, with a pre-ablation shot count of 2. A He-Ar gas carried the ablated material to the plasma chamber and then into a Thermo XseriesII Quadrupole mass spectrometer, where the following elements were analyzed: ^{7}Li, ^{11}B, ^{23}Na, ^{27}Al, ^{28}Si, ^{31}P, ^{39}K, ^{47}Ti, ^{48}Ti, ^{49}Ti, ^{55}Mn, ^{56}Fe, ^{65}Cu, ^{72}Ge, ^{85}Rb, ^{88}Sr, ^{205}Tl, ^{208}Pb. Trace element concentrations were standardized to NIST-612 (Jochum *et al.,* 2011), and ^{28}Si in stoichiometry quartz as an internal standard, using an Excel application (LaserTram, Kent *et al.,* 2004). Spot analyses that included melt or fluid inclusions or accidental analyses of other minerals (i.e. sericite in D veins) were discarded by monitoring P, Al, Si, K, Sr, Rb. NIST-616 (Jochum *et al.,* 2011) was analyzed in between unknowns as a secondary

standard. Based on the reproducibility, ^{49}Ti was preferred over ^{47}Ti and ^{48}Ti and yields a detection limit of 0.2 ppm Ti (3 sigma on background, Table 2).

Secondary Ion Mass Spectrometer (SIMS)

In situ SIMS $\delta^{18}O$ measurements were made on the CAMECA IMS 1280 ion microprobe at the University of Wisconsin-Madison WiscSIMS lab. Values standardized with bracketing analyses of UWQ-1 quartz standard (Valley and Kita, 2009) are reported in per mil (‰) relative to V-SMOW with spot-to-spot precision of <0.3‰ (see Supp. 4: Table DR4). Oxygen isotope measurements were collected along several traverses with a 1.7-1.9 nA Cs^+ primary beam. Analyses spots were ~10 μm diameter and 1 μm deep. Operating and analytical conditions are described in detail by Kita *et al.* (2009); Valley and Kita (2009); and Ferry *et al.* (2010). Secondary ^{16}O, $^{16}O^1H^-$ and $^{18}O^-$ ions were measured simultaneously using three Faraday cup detectors (C, FC2 and H1, respectively). $^{16}O^1H^-$ ions were measured for monitoring OH in quartz and contaminant such as mineral inclusions. The duration of the analyses was 3-4 minutes and the working standard was UWQ1 quartz (12.33‰ ± 0.3‰ (2 SD); ± 0.1‰ (2SE): Kelly et al. (2007), Ferry *et al.* (2014) appendix A). The working standard was measured 4-5 times before and after every 10 to 15 unknown analyses on every sample. The 2 standard deviation error for each bracketing set of the UWQ1 analyses was 0.27‰, and is considered the internal error. The raw $^{18}O/^{16}O$ ratios and $\delta^{18}O$ data were corrected to VSMOW using 83 measurements of UWQ1 during the run with a mean of 5.75‰, and errors of 2SD = 0.44‰, and 2SE = 0.05‰. These standard procedures are described by Ushikubo *et al.* (2012); Nakashima *et al.* (2013) and Tenner *et al.* (2013) and Ferry *et al.* (2014). (Table DR3).

TitaniQ geothermometry

Formation temperatures were estimated by TitaniQ geothermometry of Huang and Audétat (2012).

$$\log \mathrm{Ti\ (ppm)} = -0.27943 \cdot 10^4 / T - 660.53 \cdot (P^{0.35} / T) + 5.6459$$

T is the temperature in Kelvin
P is the temperature in Kbar

Ti activity was estimated as 1 for the hydrothermal quartz based on the presence of rutile in quartz veins, and as 0.65 for magmatic quartz based on estimates for analogous arc rocks (Walker *et al.,* 2013).

Diffusion Calculations

Isothermal diffusion expression:

a. One dimensional

$$C = C_o \operatorname{erfc}\left(\frac{X}{2\sqrt{Dt}}\right)$$

C_o is the composition of mineral region A
C is the composition at distance X in mineral region B
D is the diffusion constant
t is time
erfc = 1-erf (error function)

See Crank (1975) and Valley (2001) for additional information

b. Spherical

$$\frac{C - C_1}{C_0 - C_1} = 1 + \frac{2a}{\Pi r} \sum_{n=1}^{\infty} \frac{(-1)^n}{n} \sin\frac{n\Pi r}{a} \exp(-Dn^2\Pi^2 t/a^2)$$

C_o is the composition at the surface of the sphere
C_1 is the initial composition of the sphere
C is the composition at distance a
r is the radius of the sphere
D is the diffusion constant
t is time

See Crank (1975) for additional information

Linear cooling

$$\log S_0 = 2.504 - \frac{1}{2}\log D_0 - \log T_i + \frac{1}{2}\log E_a + \frac{1}{2}\log T + \left(26.11\frac{E_a}{T_i}\right)$$

$\log S_0$ is log of the slope
S_0 is the slope dC/dx (m)
E_a is the activation energy
D_0 is the pre-exponent fator for diffusion
T_i is the initial temperature

See Watson and Cherniak (2015) for additional information

Diffusion Constants (Arrhenius equations):

Experimental wet diffusivities are available at temperatures that overlap only with the upper range of porphyry hydrothermal quartz precipitation: 648 - 1200 °C for Ti (Cherniak *et al.,* 2007) and 515 - 850 °C for oxygen under hydrothermal conditions (Dennis, 1984). The Arrhenius equation and experimentally determined activation energies for diffusion parallel to the c-axis of quartz were used to model diffusion perpendicular to growth zones of quartz, which are mainly on $\{\mathbf{10\bar{1}1}\}$ pyramidal faces.

a. Titanium (perpendicular to c-axis)

$D_{Ti} = 7 \times 10^{-8} \exp(-273 \pm 12 \text{kJ mol}^{-1}/RT)\text{m}^2\text{sec}^{-1}$ (Cherniak *et al.,* 2007)

Experimental temperature range: 700 to 1150°C

b. Oxygen (perpendicular to c-axis)

$D_{oxygen} = 2.09 \times 10^{-11} \exp(-138.54 \pm 19.1 \text{kJ mol}^{-1}/RT)\text{m}^2\text{sec}^{-1}$ (Dennis, 1984)

Experimental temperature range: 515 to 850°C

Chi-Square goodness-of-fit test

Chi-Square (χ^2) is a standard statistical test (Borradaile, 2003) that can be used to evaluate how well a model reflects the data. We used this test to evaluate how the measured Ti and/or O contents compare with those which would be expected under the fitted diffusion model. In this way, the Chi-Square test provides an objective tool to select the model that best fits the data, instead of selecting the preferred model by a traditional and more subjective visual fit of the model to the data. The preferred model was selected in order to minimize the Chi-Square using the formula:

$$X^2 = \sum \frac{(\text{observed} - \text{expected})^2}{\text{expected}}$$

Whereas a small Chi-Square statistical test value means that the observed data fits the expected data well, a large Chi-Square statistical test means that the observed data fits the expected data in a poor manner. The absolute number of the Chi-Square test statistic has no intrinsic meaning; therefore, the goodness of fitness cannot be compared between models on different samples.

The Chi-Square test was also used to evaluate the error of each diffusion model. Minimum and maximum timescales (also expressed as ± errors of the preferred timescale), were estimated using the range of "acceptable" good fitness. The "acceptable" good fitness range is the range of timescales with similar calculated sum of Chi-Square. Outside this range, the sum of Chi-Square increases rapidly. The acceptable range can be visualized as inflexion points in the curve that results from plotting the sum of Chi-Square versus estimated timescales.

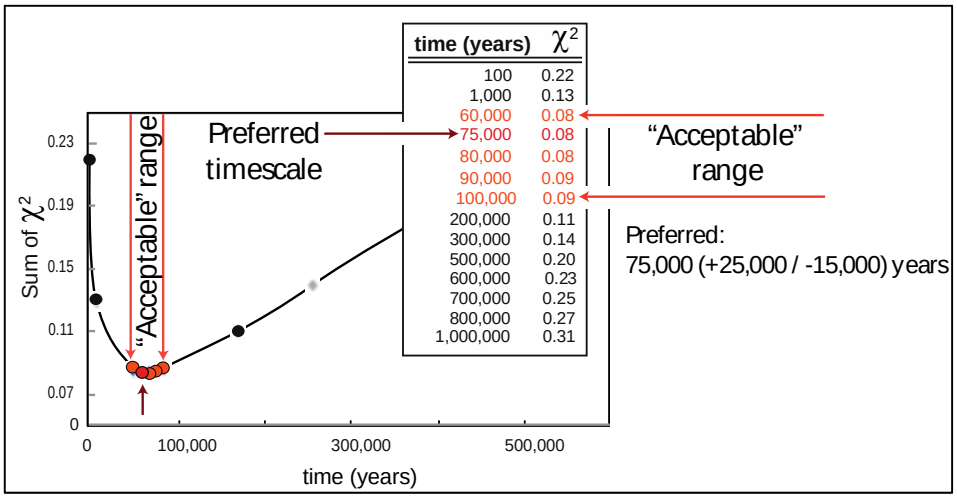

Figures

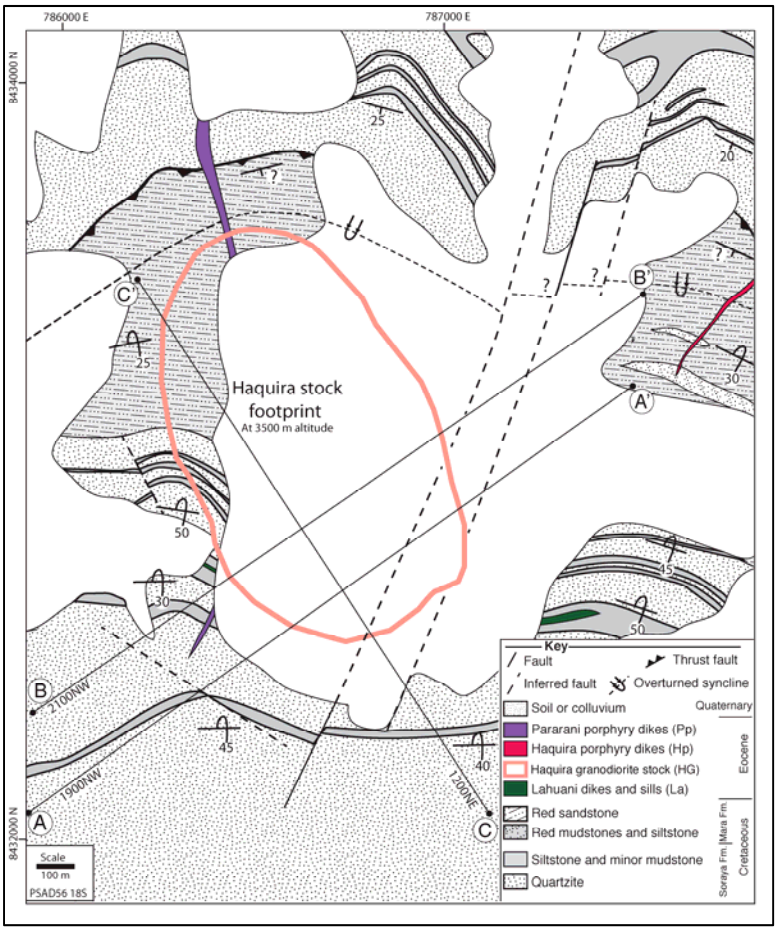

Figure DR1. Geologic map of Haquira East modified from Gans (2009) showing the location of cross-sections 1900NW, 2100NW and 1200NE (reproduced from Cernuschi, 2015). The footprint of the non-outcropping Haquira granodiorite stock is projected from a 3500 m altitude.

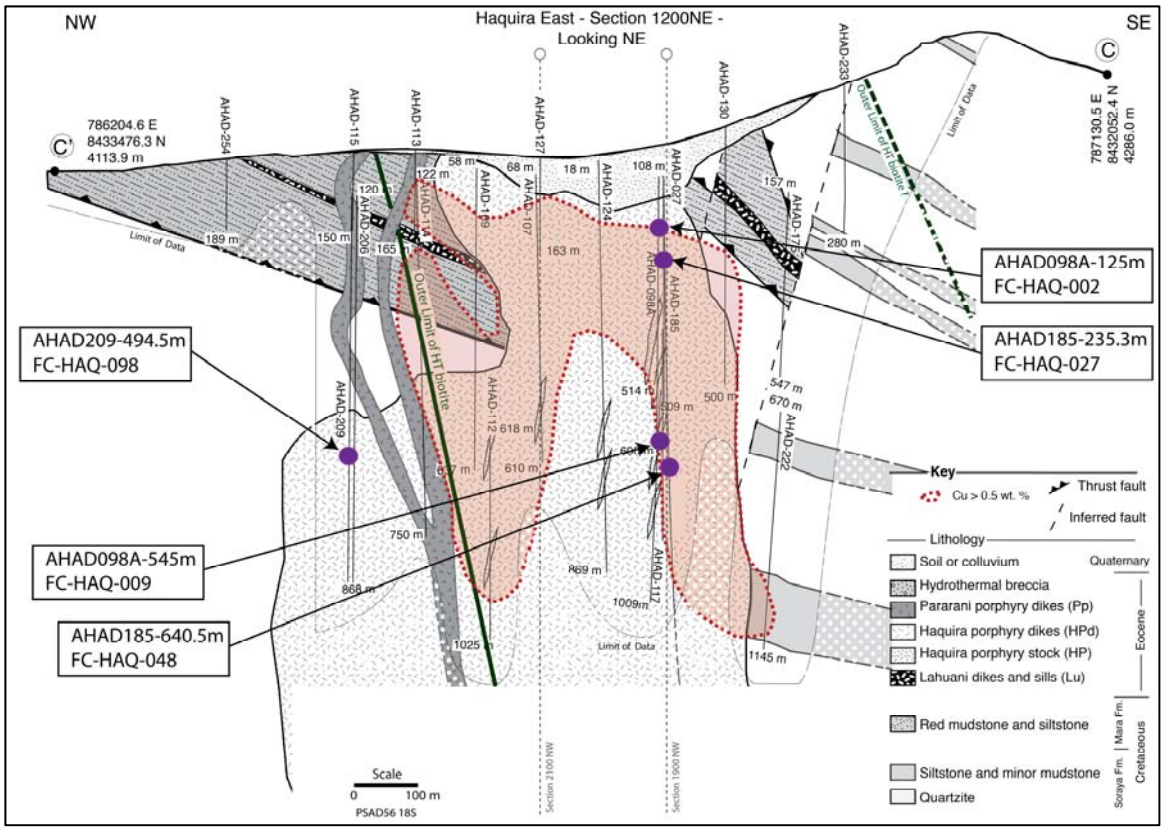

Figure DR2. Cross-section 1200NE (Cernuschi, 2015) showing location of analyzed samples in relation to the copper mineralization (>0.5 wt.% Cu) and K-silicate alteration illustrated by the extent of hydrothermal biotite after hornblende. The location of the cross-section is shown in Figure DR1.

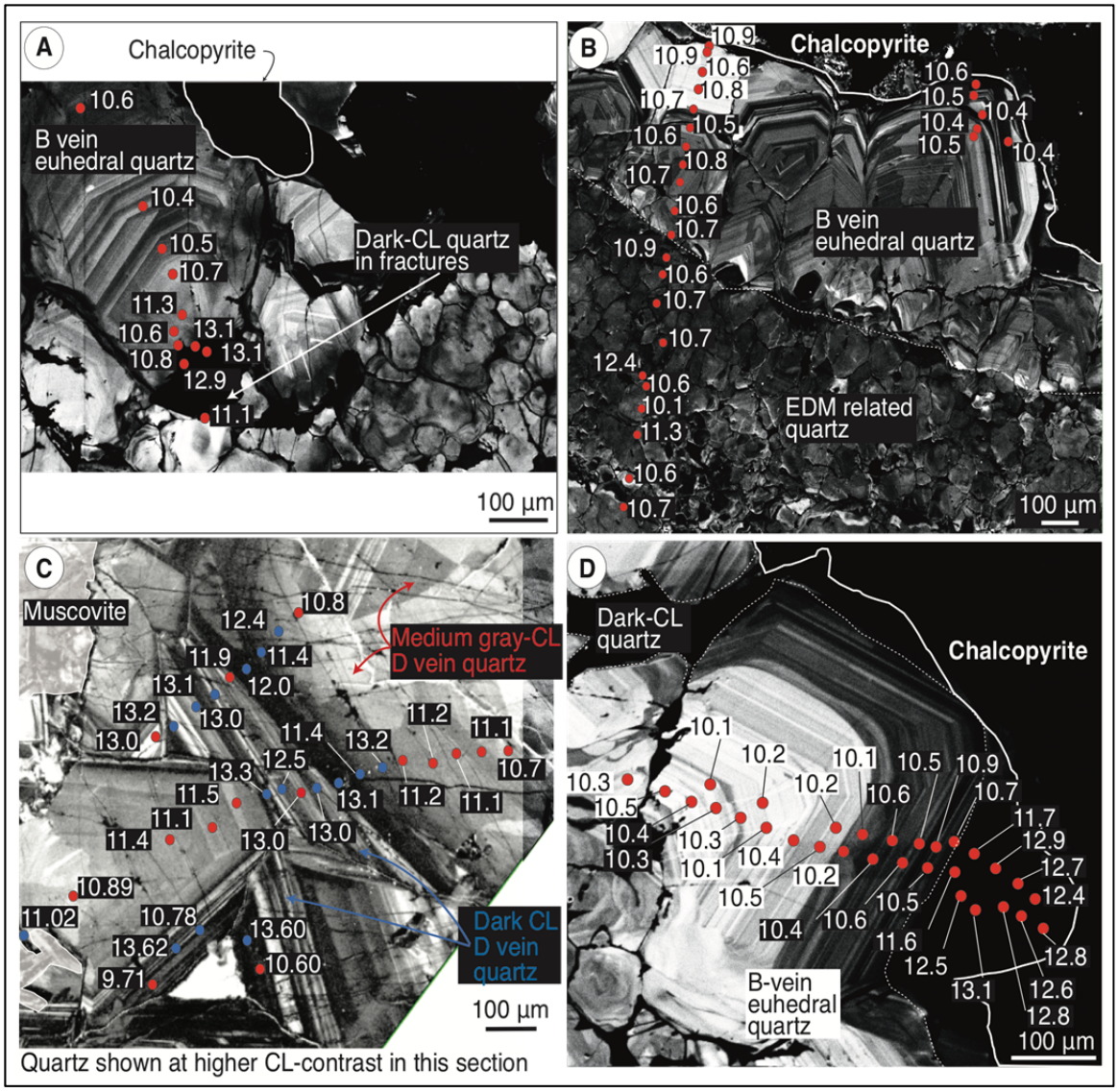

Figure DR3. $\delta^{18}O$ (‰) plotted on SEM-CL images of quartz from veins. A) B vein with chalcopyrite and late dark-CL quartz in fractures (FC-HAQ-048). B) Mosaic textured EDM related quartz overgrown by euhedral B vein quartz in contact with chalcopyrite (FC-HAQ-027). C) Euhedral quartz in D vein with medium gray-CL quartz and dark-CL quartz growth zones in contact with muscovite and pyrite (FC-HAQ-009). D) Euhedral quartz in B vein rimmed by dark-CL quartz in contact with chalcopyrite (FC-HAQ-048).

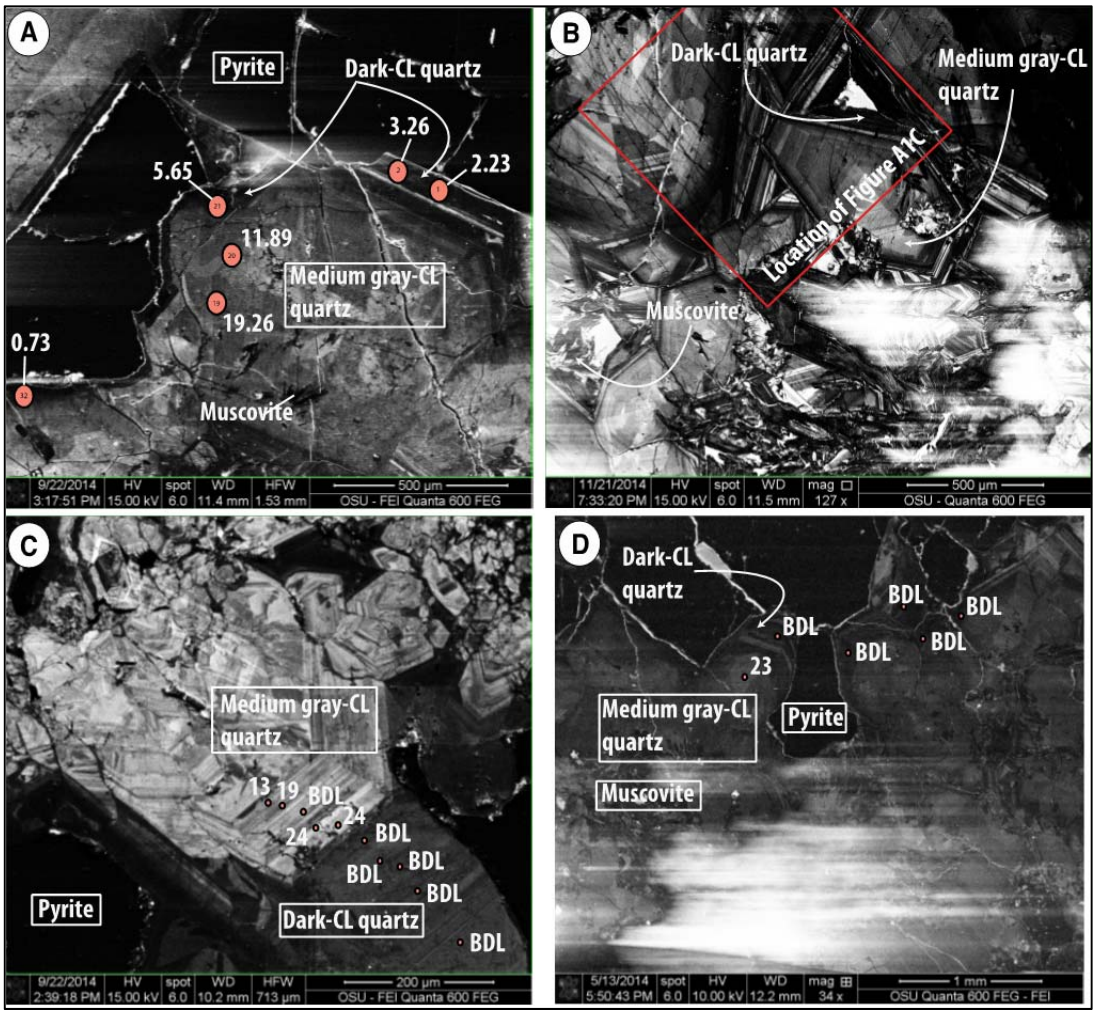

Figure DR4. Additional SEM-CL images of medium gray-CL and dark-CL quartz with muscovite and pyrite in D veins and spot location of Ti-in-Quartz data. A) FC-HAQ-098 with LA-ICP-MS spots in red showing Ti concentration. B) FC-HAQ-009, area shown in C is marked with a red square. C-D) EMP spots shown in red and indicating Ti concentration (BDL: below detection limit <13 ppm). C) FC-HAQ-098. D) FC-HAQ-009.

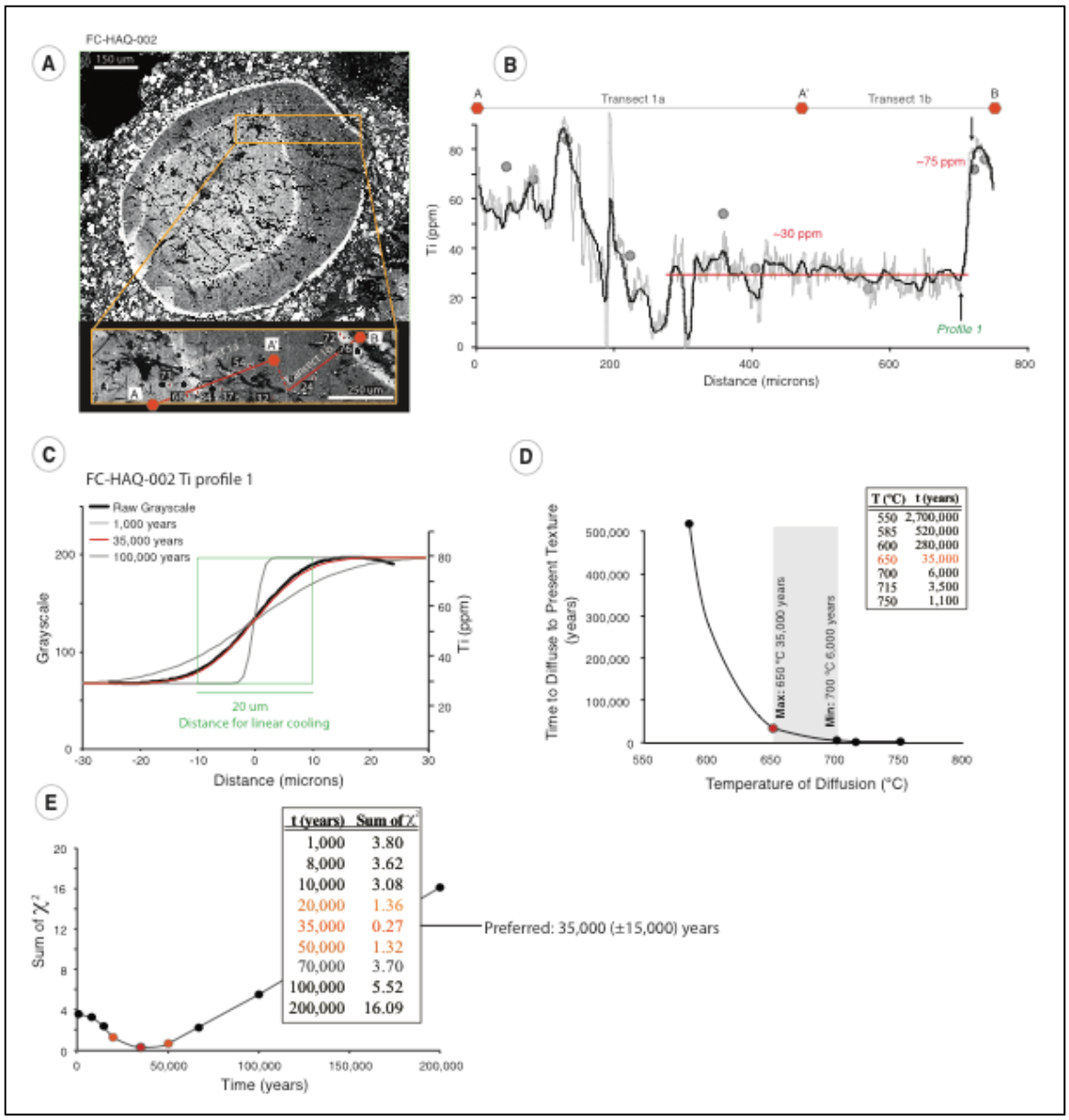

Figure DR5. A) Ti (ppm) in quartz spot analyses by EMP (Gray circles) and SEM-CL grayscale images for FC-HAQ-002. Insert shows the position of transects 1a and 1b. B) SEM-CL grayscale raw values (gray line) and smoothed grayscale (black lines) along transect 1a and 1b that are perpendicular to growth zones. Note the location of profile 1. C) Ti in quartz diffusion models for sample FC-HAQ-002 Profile 1. B) Modeled diffusion timescales versus temperature of diffusion used in the model at a fixed Sum of χ^2. The grey box shows the range of calculated diffusion timescales. The maximum timescale is the preferred. C) Sum of χ^2 versus time. The red circles show the preferred timescale based on the best fit of the model to the data as represented by the Sum of χ^2. The orange circles show the range of timescales that produce a reasonable fit of the model to the data as represented by a Sum of χ^2 smaller than 1.4.

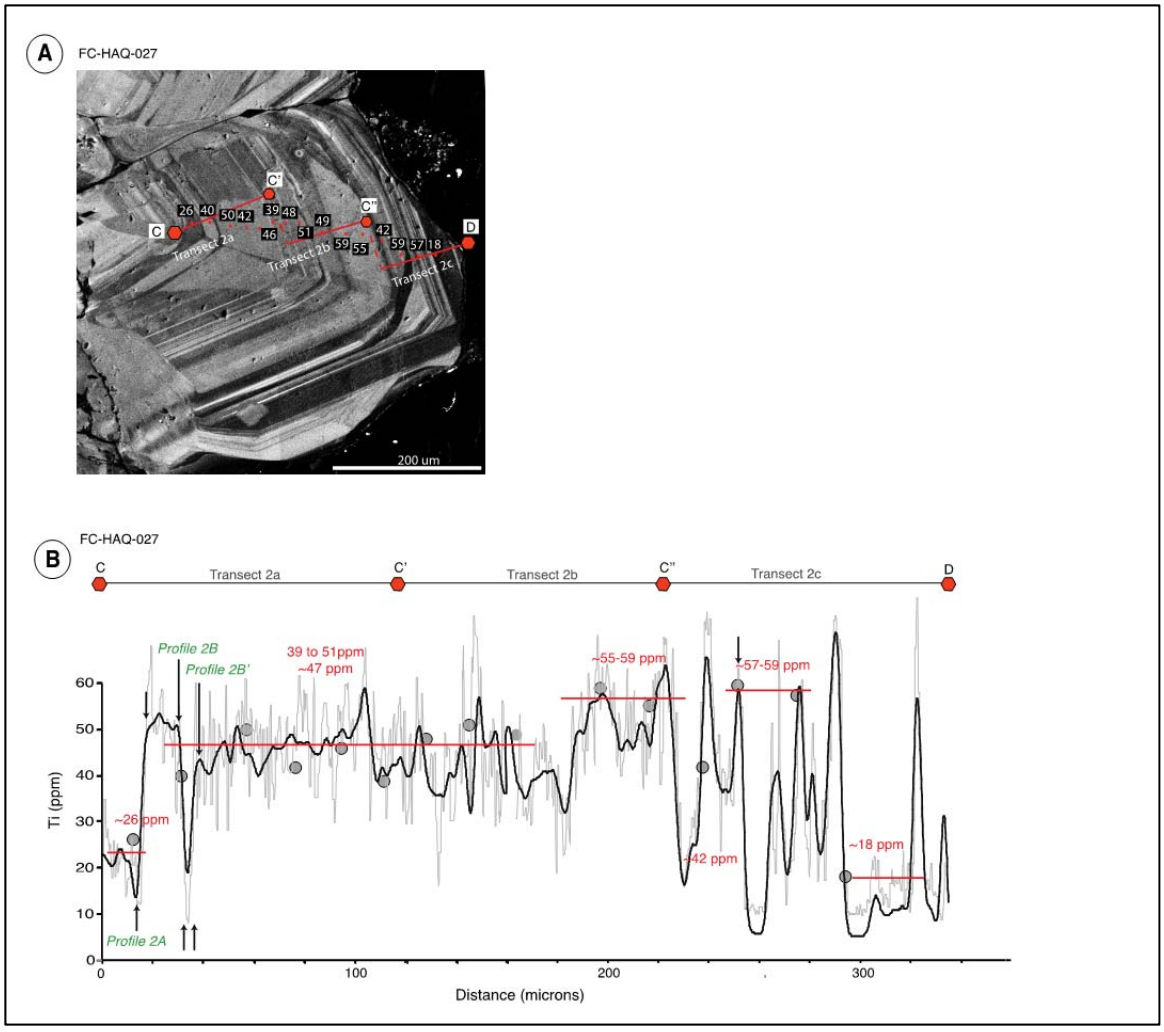

Figure DR6. A) Ti (ppm) in quartz spot analyses by EMP (Gray circles) and SEM-CL grayscale images for FC-HAQ-027. B) SEM-CL grayscale raw values (gray line) and smoothed grayscale (black lines) Note position of profiles 2A, 2B and 2B' (green-labels).

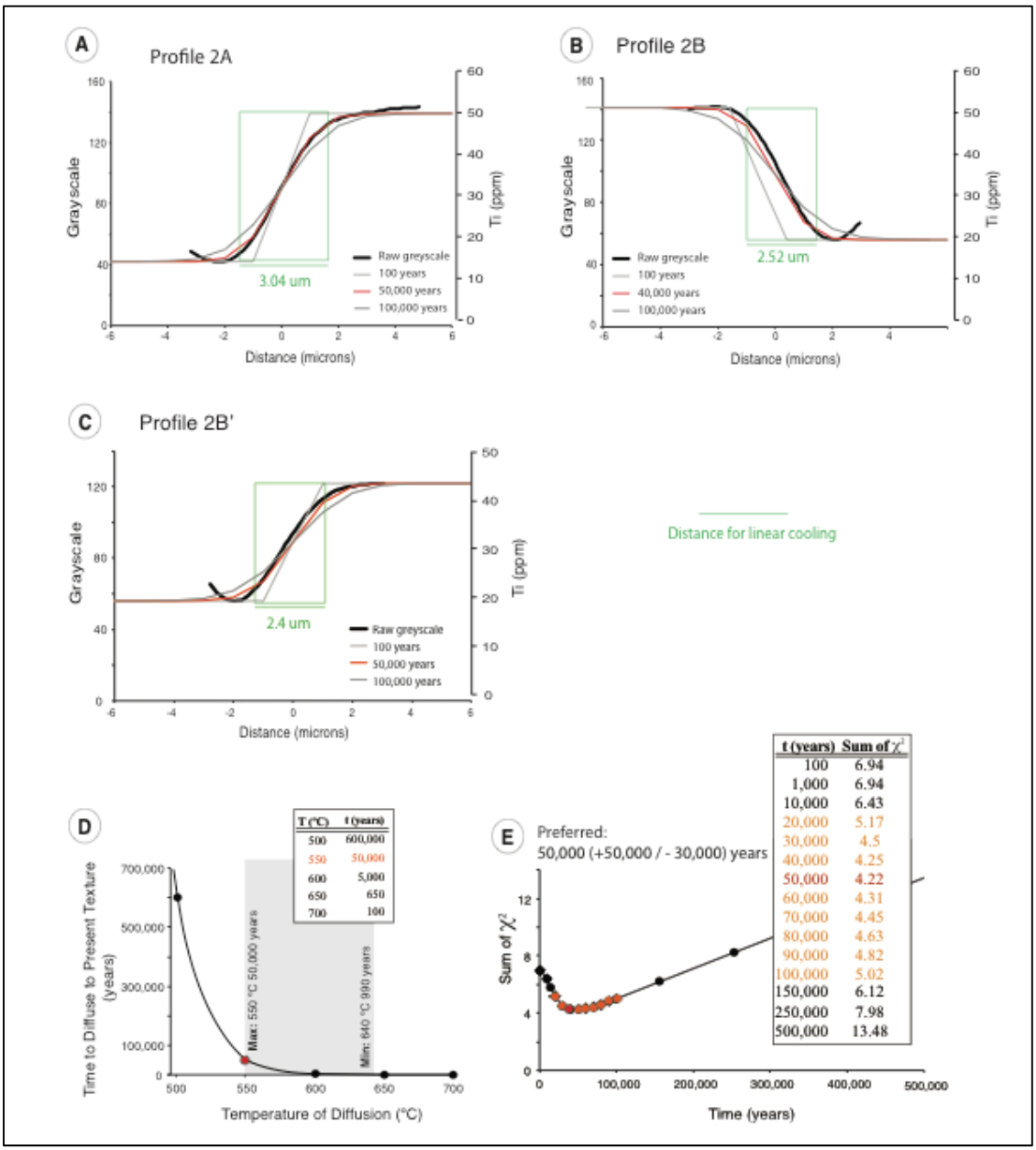

Figure DR7. Ti in quartz diffusion models for sample FC-HAQ-027 (Figure DR6): A) Profile 2A, B) Profile 2B, and C) Profile 2B´. D) Modeled diffusion timescales versus temperature of diffusion used in the model at a fixed Sum of χ^2 for model of transect 2B'. The grey box shows the range of calculated diffusion timescales. The maximum timescale is the preferred. E) Sum of χ^2 versus time, for model of transect 2B'. The red circles show the preferred timescale based on the best fit of the model to the data as represented by the Sum of χ^2. The orange circles show the range of timescales that produce a reasonable fit of the model to the data as represented by a Sum of χ^2 smaller than 5.2.

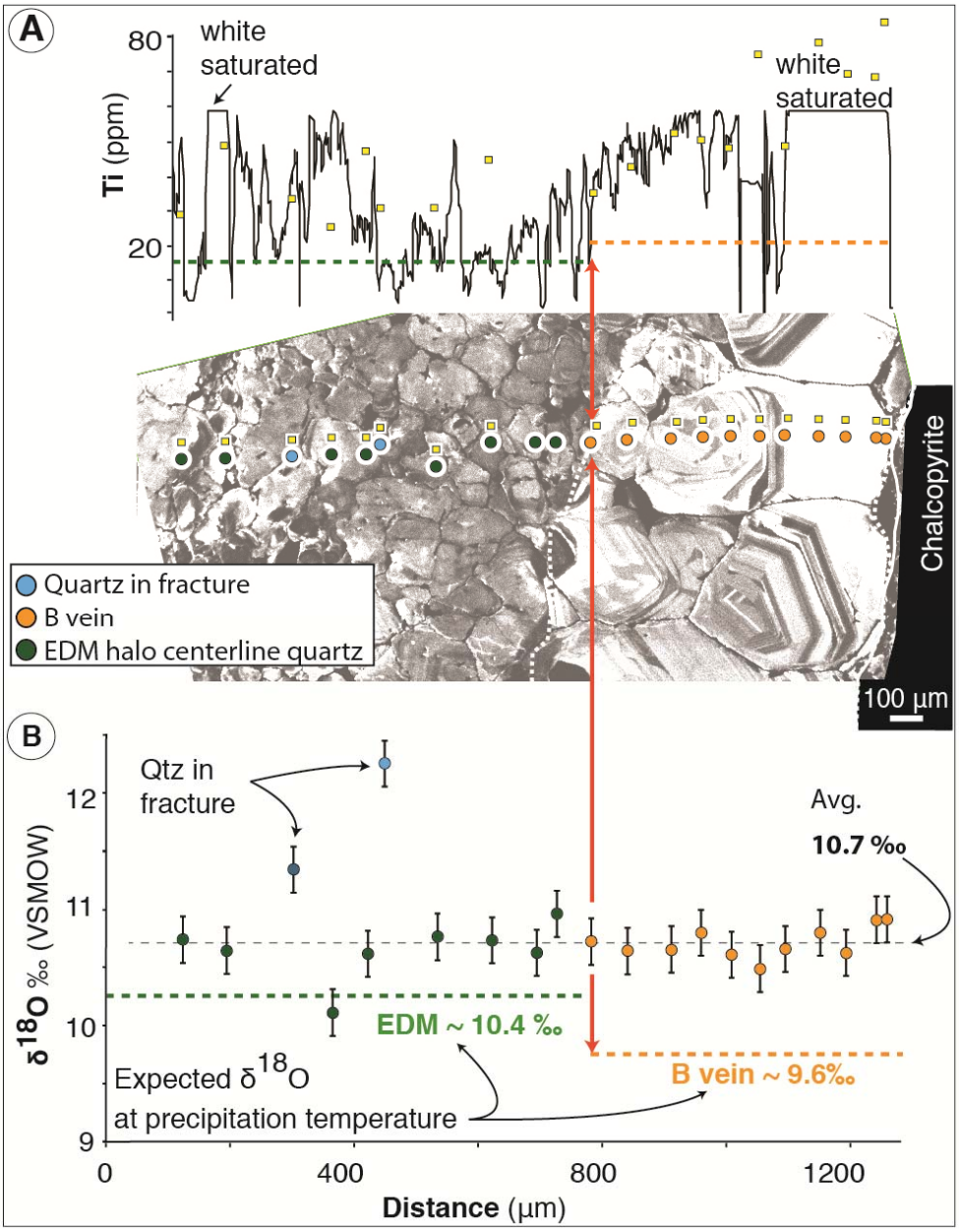

Figure DR8. Figure 3 in main text reproduced with SEM-CL image at higher contrast to highlight the fractures filled with late dark-CL quartz.

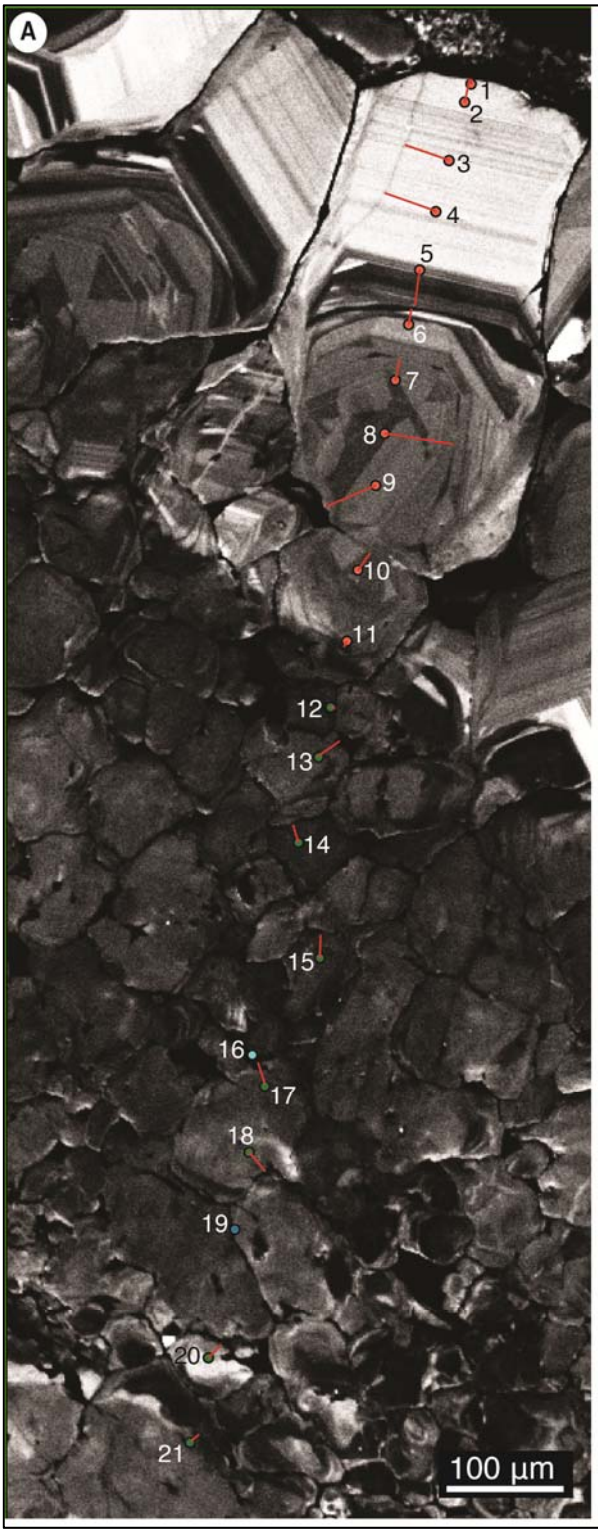

B

Spot #	$\delta^{18}O$ ‰ VSMOW	2SD	Distance (µm)
1	10.9	0.2	4
2	10.9	0.2	19
3	10.6	0.2	39
4	10.8	0.2	44
5	10.7	0.2	32
6	10.5	0.2	16
7	10.6	0.2	18
8	10.8	0.2	56
9	10.7	0.2	48
10	10.6	0.2	22
11	10.7	0.2	5
12	11.0	0.2	4
13	10.6	0.2	22
14	10.7	0.2	15
15	10.8	0.2	21
16	12.4	0.2	Fracture
17	10.6	0.2	18
18	10.1	0.2	20
19	11.3	0.2	Fracture
20	10.6	0.2	13
21	10.7	0.2	8

Figure DR9. Sample FC-HAQ-027. Distance from center of SIMS pits (see Figure DR8) to the closest fracture or dissolution band. Distance measured perpendicular from the fracture. A) SIMS pits on SEM-CL image. Pits color coded by quartz type (green = EDM, orange = B vein, light blue = late quartz in fractures (dark gray-CL and dark-CL). B) Summary table with distance to fracture or dissolution band.

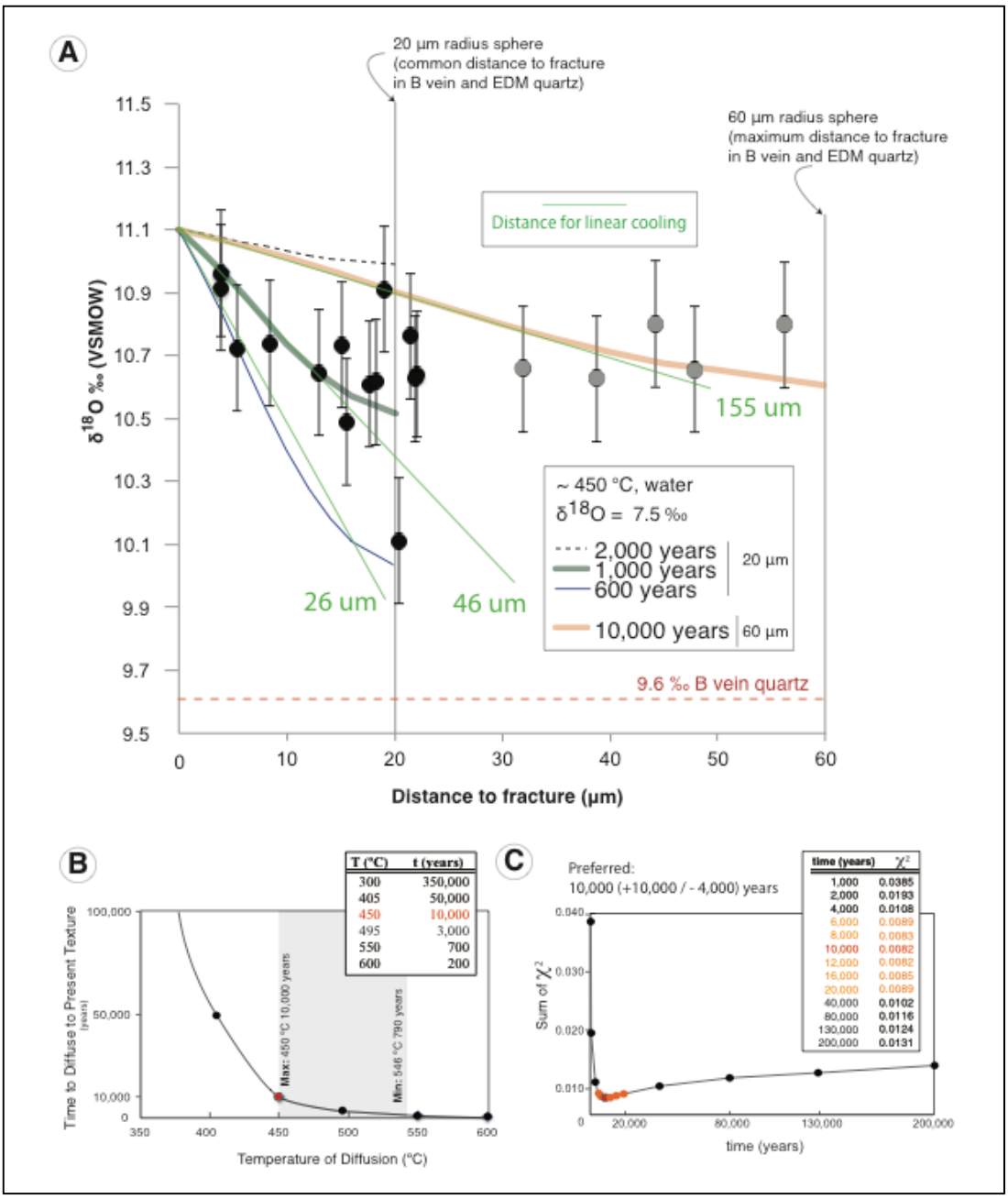

Figure DR10. A) Spherical diffusion models for partial re-equilibration of B vein and EDM quartz at 450 ºC (sample FC-HAQ-027, Figure DR8). Most of the measured distances from a SIMS-spot to the closest fractures or dissolution band are <20 µm (black dots). Partial re-equilibration can be achieved in ~1,000 years if fluid migrated through fractures spaced every 20 µm (green line). Some SIMS-spots are further away from fractures or dissolution bands. For these spots, the distances range from 20 µm to 60 µm (gray dots). These distances may be overestimates, if we assume that closely spaced fractures are present in other directions than in the observed surface. A partial re-equilibration of the quartz to the maximum measured distance to fracture (~60 µm) requires ~10,000 years (orange line). B) Modeled diffusion timescales versus temperature of diffusion used in the model at a fixed Sum of χ^2 the 10,000 year model. The grey box shows the range of calculated diffusion timescales. The maximum timescale is the preferred. C) Sum of χ^2 versus time. The red circles show the preferred timescale based on the best fit of the model to the data as represented by the Sum of χ^2. The orange circles show the range of timescales that produce a reasonable fit of the model to the data as represented by a Sum of χ^2 smaller than 0.0090.

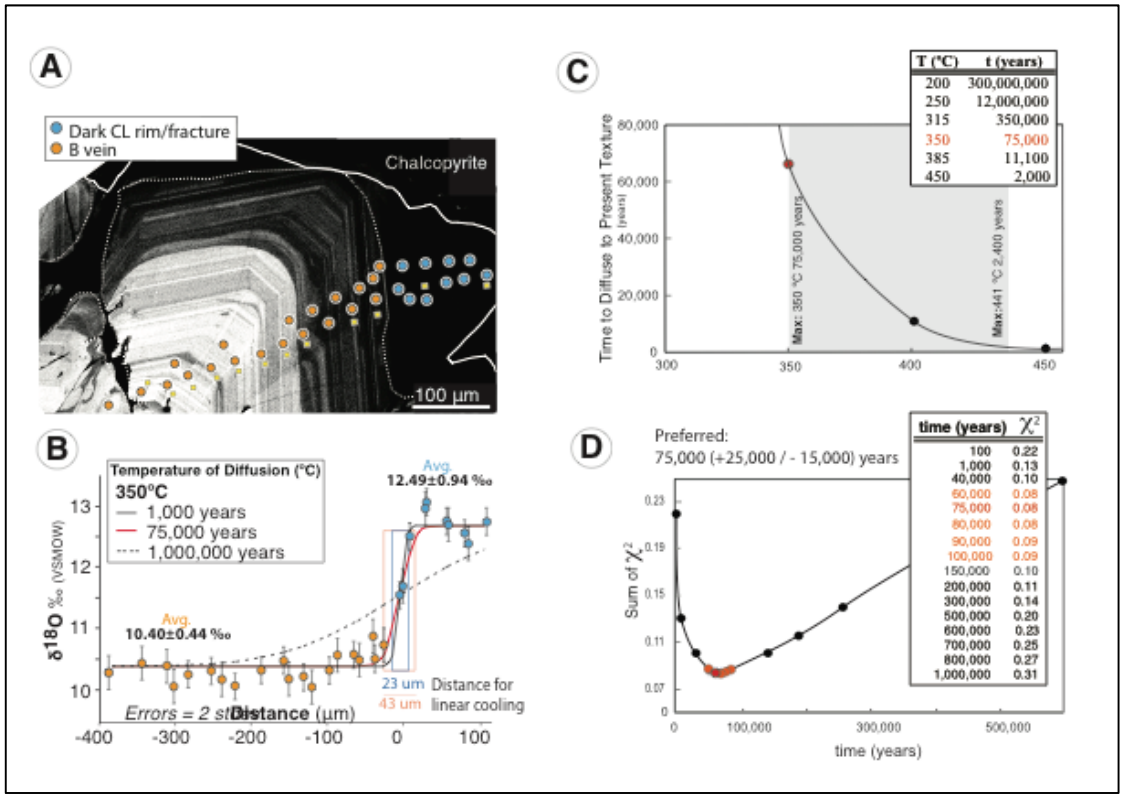

Figure DR11. A, B) Diffusion model shown in Figure 4 in the manuscript with distances used for linear cooling modelling. C) Modeled diffusion timescales versus temperature of diffusion used in the model at a fixed Sum of χ^2. The grey box shows the range of calculated diffusion timescales. The maximum timescale is the preferred. D) Sum of χ^2versus time. The red circles show the preferred timescale based on the best fit of the model to the data as represented by the Sum of χ^2. The orange circles show the range of timescales that produce a reasonable fit of the model to the data as represented by a Sum of χ^2 smaller than 0.09.

Tables

Table DR1. SAMPLE LOCATION

Sample	Drillhole	Depth (m)	Latitude	Longitude	Figure	Description
FC-HAQ-002	AHAD-098A	125.8	-14.16567	-72.34654	2	Quartz phenocryst
FC-HAQ-009	AHAD-098A	545			5	D vein
FC-HAQ-027	AHAD-185	235.3	-14.16678	-72.34653	3	EDM selvage with B vein and late quartz fractures
FC-HAQ-048	AHAD-185	640.5			4	B vein with late quartz rim
FC-HAQ-098	AHAD-209	494.5	-14.16678	-72.34653	DR4	D vein

Table DR2. TITANIUM-ALUMINUM IN QUARTZ (EMP).

Sample/Spot	Al (ppm)	Ti (ppm)	Description
Figure 2 (FC-HAQ-002)			
FC-HAQ-002-1	42	73	Gray-CL phenocryst core
FC-HAQ-002-2	47	68	Gray-CL phenocryst core
FC-HAQ-002-3	79	84	Bright-CL inner narrow zone
FC-HAQ-002-4	47	37	Gray-CL phenocryst core
FC-HAQ-002-5	43	54	Gray-CL phenocryst core
FC-HAQ-002-6	27	32	Gray-CL phenocryst core
FC-HAQ-002-7	30	24	Gray-CL phenocryst core
FC-HAQ-002-8	19	72	Bright-CL phenocryst rim
FC-HAQ-002-8	26	76	Bright-CL phenocryst rim
Figure 3 (FC-HAQ-027) Correlative to δ18O Transect 027			
FC-HAQ-027	157	84	Bright-CL banded B vein quartz
FC-HAQ-027	121	68	Bright-CL banded B vein quartz
FC-HAQ-027	84	69	Bright-CL banded B vein quartz
FC-HAQ-027	64	77	Bright-CL banded B vein quartz
FC-HAQ-027	38	47	Gray-CL banded B vein quartz
FC-HAQ-027	126	75	Bright-CL banded B vein quartz
FC-HAQ-027	100	47	Gray-CL banded B vein quartz
FC-HAQ-027	100	51	Gray-CL banded B vein quartz
FC-HAQ-027	107	53	Gray-CL banded B vein quartz
FC-HAQ-027	78	43	Gray-CL banded B vein quartz
FC-HAQ-027	28	36	Gray-CL banded B vein quartz
FC-HAQ-027	44	45	Gray-CL mosaic EDM vein quartz
FC-HAQ-027	34	31	Gray-CL mosaic EDM vein quartz
FC-HAQ-027	49	31	Gray-CL mosaic EDM vein quartz
FC-HAQ-027	54	47	Gray-CL mosaic EDM vein quartz
FC-HAQ-027	41	27	Gray-CL mosaic EDM vein quartz
FC-HAQ-027	48	33	Gray-CL mosaic EDM vein quartz
FC-HAQ-027	35	49	Gray-CL mosaic EDM vein quartz
FC-HAQ-027	60	34	Gray-CL mosaic EDM vein quartz

Sample/Spot	Al (ppm)	Ti (ppm)	Description
Figure 4 (FC-HAQ-048) Correlative to δ18O Transect 048			
FC-HAQ-048	BDL	BDL	Dark-CL quartz rim
FC-HAQ-048	BDL	BDL	Dark-CL quartz rim
FC-HAQ-048	97	39	Gray-CL banded B vein quartz
FC-HAQ-048	23	49	Gray-CL banded B vein quartz
FC-HAQ-048	45	59	Gray-CL banded B vein quartz
FC-HAQ-048	55	79	Bright-CL banded B vein quartz
FC-HAQ-048	59	65	Bright-CL banded B vein quartz
FC-HAQ-048	115	98	Bright-CL banded B vein quartz
FC-HAQ-048	80	92	Bright-CL banded B vein quartz
FC-HAQ-048	123	105	Bright-CL banded B vein quartz
FC-HAQ-048	278	114	Bright-CL banded B vein quartz
FC-HAQ-048	250	109	Bright-CL banded B vein quartz
Data Repository Figure DR4a-c (FC-HAQ-098)			
FC-HAQ-098-1	1602	13	Medium gray-CL quartz D vein
FC-HAQ-098-2	793	19	Medium gray-CL quartz D vein
FC-HAQ-098-3	1085	BDL	Medium gray-CL quartz D vein
FC-HAQ-098-4	2043	24	Medium gray-CL quartz D vein
FC-HAQ-098-5	644	24	Medium gray-CL quartz D vein
FC-HAQ-098-6	197	BDL	Dark CL-quartz D vein
FC-HAQ-098-7	19	BDL	Dark CL-quartz D vein
FC-HAQ-098-8	1303	BDL	Dark CL-quartz D vein
FC-HAQ-098-9	215	BDL	Dark CL-quartz D vein
Data Repository Figure DR4b-d (FC-HAQ-009)			
FC-HAQ-009-2	125	23	Medium gray-CL quartz D vein
FC-HAQ-009-4	161	BDL	Dark CL-quartz D vein
FC-HAQ-009-5	77	BDL	Dark CL-quartz D vein
FC-HAQ-009-7	45	BDL	Dark CL-quartz D vein
FC-HAQ-009-10	193	BDL	Dark CL-quartz D vein
FC-HAQ-009-12	91	BDL	Dark CL-quartz D vein

Table DR2. (Cont.)

Sample/Spot	Al (ppm)	Ti (ppm)	Description
Data Repository Figure DR6a-b			
FC-HAQ-027-b1	63	26	Gray-CL banded B vein quartz
FC-HAQ-027-b2	125	40	Gray-CL banded B vein quartz
FC-HAQ-027-b3	152	50	Gray-CL banded B vein quartz
FC-HAQ-027-b4	203	42	Gray-CL banded B vein quartz
FC-HAQ-027-b5	189	46	Gray-CL banded B vein quartz
FC-HAQ-027-b6	162	39	Gray-CL banded B vein quartz
FC-HAQ-027-b7	191	48	Gray-CL banded B vein quartz
FC-HAQ-027-b8	218	51	Gray-CL banded B vein quartz
FC-HAQ-027-b9	177	49	Gray-CL banded B vein quartz
FC-HAQ-027-b10	190	59	Gray-CL banded B vein quartz
FC-HAQ-027-b11	179	55	Gray-CL banded B vein quartz
FC-HAQ-027-b12	111	42	Gray-CL banded B vein quartz
FC-HAQ-027-b13	101	59	Gray-CL banded B vein quartz
FC-HAQ-027-b14	612	57	Gray-CL banded B vein quartz
FC-HAQ-027-b15	82	18	Gray-CL banded B vein quartz

Spot	Al (ppm)	Ti (ppm)
Shandong Standard		
1	145	57
1	146	60
3	146	62
4	131	57
5	138	59
6	130	53
7	133	56
8	131	55
9	130	58
10	131	57
11	132	56
12	132	65
13	130	57
14	129	54
15	132	59
16	121	59
17	128	55
18	128	64
Average:	**133**	**58**
2 Stdev:	**7**	**6**
Preferred values	Audetat *et al.*, 2015	
Average:	**154**	**57**
2 stdev:	**15**	**4**

Table DR3. TRACE ELEMENTS IN QUARTZ (LA-ICP-MS).

Sample	Al (ppm)	Li (ppm)	^{49}Ti (ppm)	Ge (ppm)	Quartz type
Data Repository Figure DR4b (FC-HAQ-009)					
FC-HAQ-009-20	49.09	-	11.89	0.79	Medium gray-CL D vein
FC-HAQ-098-22	539.14	4.84	12.90	0.73	Medium gray-CL D vein
FC-HAQ-009-19	123.00	1.02	19.26	1.34	Medium gray-CL D vein
Average:	**237.08**	**2.93**	**14.68**	**0.95**	
2 stdev:	**528.38**	**5.40**	**7.99**	**0.67**	
Data Repository Figure DR4a (FC-HAQ-098)					
FC-HAQ-009-1	684.68	5.75	2.23	1.07	Dark-CL D vein
FC-HAQ-009-2	559.36	3.35	3.26	1.00	Dark-CL D vein
FC-HAQ-009-21	45.07	0.77	5.65	1.32	Dark-CL D vein
FC-HAQ-009-32	240.17	2.62	0.73	1.79	Dark-CL D vein
Average:	**382.32**	**3.12**	**2.97**	**1.30**	
2 stdev:	**585.05**	**4.13**	**4.13**	**0.72**	

Standard	Al (ppm)	Li (ppm)	^{49}Ti (ppm)	Ge (ppm)
NISTSRM616-1	10751.43	0.95	1.83	0.20
NISTSRM616-2	11415.58	0.91	1.70	0.24
NISTSRM616-3	11734.98	0.81	1.93	0.25
NISTSRM616-4	10471.51	0.91	1.59	0.28
NISTSRM616-4b	11819.21	0.90	2.23	-
NISTSRM616-7	11850.67	0.82	2.75	0.24
NISTSRM616-8	10957.49	0.87	2.05	0.17
NISTSRM616-9	11432.72	0.79	1.83	0.23
NISTSRM616-10	11462.42	1.02	2.26	0.20
NISTSRM616-12	11071.23	1.05	2.23	0.21
NISTSRM616-13	11149.52	0.85	2.06	0.40
Average:	**11283.34**	**0.90**	**2.04**	**0.24**
2 stdev:	**893.52**	**0.17**	**0.65**	**0.13**
NISTSRM616 preferred values			Jochum *et al.*, 2011	
Average:		**0.895**	**2.65**	**0.283**
2 stdev:		**0.059**	**0.29**	**0.039**

Table DR4. $\delta^{18}O$ (V-SMOW) OF QUARTZ (SIMS).

Comment	$\delta^{18}O$ ‰ VSMOW	2SD (ext.)	Number Analys.
(Figure 3) FC-HAQ-027			
027 B vein	10.91	0.20	
027 B vein	10.91	0.20	
027 B vein	10.63	0.20	
027 B vein	10.80	0.20	
027 B vein	10.66	0.20	
027 B vein	10.49	0.20	
027 B vein	10.61	0.20	
027 B vein	10.80	0.20	
027 B vein	10.65	0.20	
027 B vein	10.64	0.20	
027 B vein	10.72	0.20	
Mean, B vein quartz	**10.71**	**0.26**	11
027 EDM	10.96	0.20	
027 EDM	10.63	0.20	
027 EDM	10.73	0.20	
027 EDM	10.76	0.20	
027 Dark-CL fracture	***12.39***	0.20	
027 EDM	10.62	0.20	
027 EDM	10.11	0.20	
027 Medium-CL fracture	***11.32***	0.20	
027 EDM	10.64	0.20	
027 EDM	10.74	0.20	
027 EDM	10.78	0.20	
Mean, EDM quartz - All	***10.66***	***0.46***	11
027 B vein	10.59	0.20	
027 B vein	10.49	0.20	
027 B vein	10.39	0.20	
027 B vein	10.44	0.20	
027 B vein	10.48	0.20	
027 B vein	10.36	0.20	
027 B vein	10.84	0.20	
027 B vein	10.85	0.20	
Mean, B vein quartz	**10.55**	**0.39**	8
Mean, B vein quartz - All	***10.64***	***0.35***	19
All EDM and B vein in FC-HAQ-027	**10.67**	**0.36**	

Comment	$\delta^{18}O$ ‰ VSMOW	2SD (ext.)	Number Analys.
(Figure 4) FC-HAQ-048			
048 Late dark CL quartz	12.75	0.22	
048 Late dark CL quartz	12.57	0.22	
048 Late dark CL quartz	12.76	0.22	
048 Late dark CL quartz	13.07	0.22	
048 Late dark CL quartz	12.52	0.22	
048 Late dark CL quartz	11.57	0.22	
Mean, Late dark CL quartz	**12.54**	**1.03**	6
048 B vein	10.54	0.22	
048 B vein	10.61	0.22	
048 B vein	10.35	0.22	
048 B vein	10.24	0.22	
048 B vein	10.51	0.22	
048 B vein	10.36	0.22	
048 B vein	10.10	0.22	
048 B vein	10.34	0.22	
048 B vein	10.29	0.22	
048 B vein	10.42	0.27	
048 B vein	10.47	0.27	
048 B vein	10.31	0.27	
Mean, B vein quartz	**10.38**	**0.28**	12
048 Late dark CL quartz	12.40	0.27	
048 Late dark CL quartz	12.71	0.27	
048 Late dark CL quartz	12.96	0.27	
048 Late dark CL quartz	11.71	0.27	
Mean, Late dark CL quartz	**12.44**	**1.08**	4
048 B vein	10.76	0.27	
048 B vein	10.90	0.27	
048 B vein	10.52	0.27	
048 B vein	10.60	0.27	
048 B vein	10.08	0.27	
048 B vein	10.21	0.27	
048 B vein	10.20	0.27	
048 B vein	10.09	0.27	
Mean, session 2 B vein quartz	**10.42**	**0.63**	8
Mean, B vein quartz - All	***10.40***	***0.44***	20
Mean, Late dark CL quartz -All	***12.49***	***0.94***	10

Comment	$\delta^{18}O$ ‰ VSMOW	2SD (ext.)	Number Analys.
(Figure 5) FC-HAQ-009	session 1		
009 D-vein, medium gray-CL	9.71	0.32	
009 D-vein, dark-CL	13.62	0.32	
009 D-vein, dark-CL	10.78	0.32	
009 D-vein, dark-CL	13.60	0.32	
009 D-vein, medium gray-CL	10.60	0.32	
009 D-vein, medium gray-CL	11.49	0.32	
009 D-vein, medium gray-CL	11.13	0.32	
009 D-vein, medium gray-CL	11.38	0.32	
009 D-vein, medium gray-CL	10.89	0.32	
009 D-vein, dark-CL	11.02	0.32	
Mean, medium gray-CL session	***11.52***	***1.30***	6
Mean, dark-CL session 1	***12.26***	***3.14***	4
	session 2		
009 D-vein, dark-CL	13.34	0.22	
009 D-vein, dark-CL	12.53	0.22	
009 D-vein, dark-CL	13.01	0.22	
009 D-vein, dark-CL	12.93	0.22	
009 D-vein, dark-CL	13.10	0.22	
009 D-vein, dark-CL	11.39	0.22	
009 D-vein, dark-CL	13.15	0.25	
009 D-vein, medium gray-CL	11.18	0.25	
009 D-vein, medium gray-CL	11.19	0.25	
009 D-vein, medium gray-CL	11.09	0.25	
009 D-vein, medium gray-CL	11.13	0.25	
009 D-vein, medium gray-CL	10.69	0.25	
009 D-vein, medium gray-CL	12.98	0.25	
009 D-vein, dark-CL	13.15	0.25	
009 D-vein, dark-CL	13.02	0.25	
009 D-vein, dark-CL	13.14	0.25	
009 D-vein, medium gray-CL	11.91	0.25	
009 D-vein, dark-CL	12.02	0.25	
009 D-vein, dark-CL	11.43	0.25	
009 D-vein, dark-CL	12.41	0.25	
009 D-vein, medium gray-CL	10.84	0.25	
Mean, medium gray-CL session	***11.16***	***1.45***	8
Mean, dark-CL session 2	***12.57***	***1.82***	13
Mean, medium gray-CL -all	***11.16***	***1.45***	14
Mean, dark-CL session -all	***12.57***	***1.82***	17

Table DR4. (Cont.)

Comment	$\delta^{18}O$ ‰ VSMOW	2SD (ext.)	Number Analys.
(Figure DR4a) FC-HAQ-004			
004 Late dark CL quartz	13.14	0.22	
004 B vein	10.66	0.22	
004 B vein	10.46	0.22	
004 B vein	10.43	0.22	
004 B vein	10.61	0.22	
004 B vein	10.51	0.22	
004 B vein	12.88	0.22	
004 B vein	10.79	0.22	
004 B vein	10.62	0.22	
004 Late dark CL quartz	13.08	0.22	
004 Late dark CL quartz	11.28	0.22	
004 Late dark CL quartz	11.05	0.22	
004 B vein	10.74	0.22	
Mean, B vein quartz - All	***10.86***	***1.54***	9
Mean, Late dark CL quartz -All	***12.14***	***2.25***	4
All standards			
UWQ-1 garnet	**Mean** **5.757**	**2 sdev** **0.302**	53

Averages all of assays by quartz type

			2SD (ext.)	Number Analys.
EDM quartz	**Max.**	11.10		
	Avg.	**10.66**	**0.44**	9
	Min.	10.23		
B vein quartz	**Max.**	11.39		
	Avg.	**10.58**	**0.81**	48
	Min.	9.77		
Medium gray-CL quartz in D vein	**Max.**	12.61		
	Avg.	**11.16**	**1.45**	14
	Min.	9.71		
Medium gray-CL quartz in fractures		11.32	**0.20**	1
Medium gray-CL quartz in D vein and fractures	**Max.**	12.61		
	Avg.	**11.17**	**1.40**	15
	Min.	9.71		
Dark CL quartz in D vein	**Max.**	14.39		
	Avg.	**12.57**	**1.82**	17
	Min.	10.75		
Dark CL quartz in rims and fractures	**Max.**	13.07		
	Avg.	**12.40**	**1.45**	15
	Min.	11.57		
Dark CL quartz in D veins, rims and fractures	**Max.**	14.39		
	Avg.	**12.49**	**1.60**	32
	Min.	10.75		

Table DR5. PORPHYRY AND VEIN FORMATION TEMPERATURES BASED ON PHASE EQUILIBRIA, TITANIQ GEOTHERMOMETER AND FLUID INCLUSION DATA

Table A5. PORPHYRY AND VEIN FORMATION TEMPERATURES BASED ON PHASE EQUILIBRIA, TITANIQ GEOTHERMOMETER AND FLUID INCLUSION DATA

Quartz type	T(°C) [phase]	Ti (ppm)	T(ºC) [Ti] T (ºC)	P (kbar)	αTiO2	T(°C) [pref. min.]
Igneous (gray-CL)	650-700	24-54	650-737	3.0 L.	0.65	650
B (gray-CL)	550-600	18-59	543-640	1.4 L.	1.0	550
EDM (gray-CL)	500-550	27-49	566-621	1.4 L.	1.0	500
D (medium gray-CL)	450-500	13–25	494-546	1.1 L.-H.	1.0	450
D (dark-CL)	350-450	1–6	343-441	1.1 L.-H.	1.0	350

Notes: T (ºC) [phase] was estimated based on the phase stability of quartz – K-feldspar – Muscovite – Andalusite (Seedorff *et al.,* 2005). **T (ºC)** [Ti] was calculated using the Ti-in-Q geothermometer (Huang and Audétat, 2012) of the lowest Ti zones, together with pressure constraints from fluid inclusion and hornblende barometry (Cernuschi *unpub.*). P (kbar) = Pressure in kbars, L. = Lithostatic, H. = Hydrostatic, αTiO_2 = Titanium activity. **T (ºC) [pref. min.]** is the preferred minimum formation temperature used for the diffusion modeling.

Table DR6. DIFFUSION TIMESCALES.

Stage	Alteration	Diffusion	D (m^2/s)	Estimated Temperature (ºC) Min. -Preferred-	Max.	Calculated Timescale (years) Min. from Max. T(ºC)	Max. from Min. T(ºC) - Preferred -	Error for Max. estimate (based on Chi-Square) (-)	(+)
1: Magmatic and main Cu-Mo stage	K-silicate	1D Ti	$2.50x10^{-23}$	650	700	6,000	**35,000**	15,000	15,000
2: Second Cu-Mo stage	K-silicate	1D Ti	$3.32x10^{-25}$	550	640	990	**50,000**	30,000	50,000
3: 450ºC δ18O homogenization of early high temperature quartz	Sericitic	3D (20 um) $\delta^{18}O$	$2.14x10^{-21}$	450	546	1,200	**10,000**	4,000	10,000
		3D (60 um) $\delta^{18}O$				300	**1,000**		
						790	**10,000**		
4: Late quartz in D veins and fractures	Sericitic	1D Ti	$5.38x10^{-23}$	350	441	2,400	**75,000**	15,000	25,000
Total:						***10,590***	***170,000***	***64,000***	***100,000***

Note: Ppy = porphyry, Ap = aplite, DQ = deep quartz veins, EDM = early dark micaceous halos, BMQ = banded molybdenite quartz veins. Min. = Minimum, Max. = Maximum. Minimum calculated timescale based on maximum estiamted temparature. Maximum calculated timescale based on minimum estimated temperature. The maximum timescale is the preferred timescale. The error of the preferred timescale is based on the error of the Chi-Square goodness of fitness. 1D = one dimensional diffusion. 3D=spherical diffusion, sphere radius in microns reflects the spacing of fractures in quartz.

Table DR7. LINEAR COOLING SUMMARY.

Stage	*Isothermal conditions* T (°C) (estimated)	Time (yr)	Model type	Transect	*Linear Cooling** *T range* (for calc.)	Cooling Rate °/ yr	°/1,000 yr	Length Dif. Prof. d (μm)	Time (yr) (for T range)
1: Magmatic and main Cu-Mo stage	650	**35,000**	1D	FC-HAQ-002	700-550	0.0067	6.7		22,400
					700-600	0.0067	6.7	20	14,900
					675-600	0.00272	2.7		**27,600**
2: Second Cu-Mo stage	550	**50,000**	1D	FC-HAQ -027 2A	600-475	0.00306	3.1	3.04	**40,900**
		40,000	1D	2B	600-475	0.00448	4.5	2.52	27,900
		50,000	1D	2B'	**600-475**	0.00493	4.9	2.04	25,400
3: 450°C $\delta^{18}O$ homogenization of early high temperature quartz	450	**10,000**	1D	FC-HAQ-027	475-425	0.00657	6.6		7,600
	450	**10,000**	3D		475-400	0.00657	6.6	92	11,400
					475-375	0.00657	6.6		**15,200**
					450-350	0.0028	2.8		35,000
4: Late quartz in D veins and fractures	350	**75,000**	1D	FC-HAQ-048	375-325	0.00254	2.5	23	20,000
					375-325*	*0.0007*	*0.7*	*43*	***69,000***
Total Cooling time (Min)					700-325°C			Estimate #1	75,500
Total Cooling time (Max)	**650-350°C**	**170,000**			**675-325°C, excludes ****			Estimate #2	**103,700**
Total Cooling time (Max)					***675-325°C***			Estimate #3	***152,700***

***Linear Cooling Calculation**: Linear cooling is estimated using the formulation and equations of Watson and Cherniak (2015). See details in page 7. For each diffusion profile, the slope of the diffusion profile, So, was calculated the midpoint of the diffusion profile. The intercept of the slope with the upper Ti concentration (Ch) and lower Ti concentration (Co) at infinite distance provides a diffusion length, d (μm) (see Fig. 1 of Cherniak and Watson, 2015). Using the measured diffusion length, So (%/m) = [100%/d (μm)]*10exp(-6) μm/m. The cooling rate (°/s) (shown above in °C/yr and °C/1000 yr) can be solved by iteration using the diffusivity parameters (Ea, Do) for Ti and O in quartz and the initial temperature from the observed log(So) using the equation of Watson and Cherniak (2015). The total time (yr) from estimated initial to final temperature of each Stage can then be calculated. Note that for cooling from initial magmatic temperatures (~700°C) to low temperature hydrothermal conditions (325°C), we choose 700-600°C for Stage 1 and 475-375°C for Stage 3. This allows continual thermal cooling (without overlap or gaps in temperature intervals). Nonetheless, during each of these individual cooling intervals (Stages 1 to 4), there may have been one or more heating events followed by cooling, and the modeled linear cooling rate in the interval therefore represents an average cooling rate for the interval. Total cooling time estimates using linear cooling are less than isothermal cooling because diffusion occurs most rapidly at higher temperatures of the cooling interval (this also means that we can neglect diffusion at lower temperature stages, i.e., diffusion in Stages 2, 3, and 4 has negligible effects on the diffusion profile established in Stage 1 (700-600°C). Cooling rates using these estimates are relatively uniform at 2.5 to 6.7°C/1000 yr, excepting the 0.7°C/1000 yr Stage 4 estimate for the 43 μm wide diffusion profile. This latter is considered likely to be too low a cooling rate, as convective cooling by groundwater will likely accelerate cooling below 375°C; alternatively, regional cooling at great depth at Haquira may cause a slowing of cooling rates to 2.5 °C/1000 yr. Therefore, linear estimate #3 (152,700 yr) is not likely, and estimates #1 and #2 provide a minimum and maximum cooling time from 675-700°C to 325°C. We note that the three time estimates of 14,900 to 27,600 yr for Stage 1 provide an estimate for the duration of magmatic intrusions associated with the Cu-Mo ores.

Table DR8. ESTIMATED FORMATION TEMPERATURES BASED ON MEASURED OXYGEN ISOTOPIC COMPOSITION OF QUARTZ AND DIFFERENT FRACTIONATION FACTORS.

Quartz type	T(°C) [preferred minimum estimate]	T (°C) estimates from $\delta^{18}O$ ‰ data									
		Measured $\delta^{18}O$ ‰ in quartz		Frac. factor Matsuhisa *et al.*, 1979 (250 - 500 °C) *	T (°C)	Frac. factor Zhang *et al.*, 1989 (180 - 550 °C) *	T (°C)	Frac. factor Hu & Clayton, 2003 (450 - 700 °C) *	T (°C)
Late dark-CL quartz	350	Max.	14.39	Magmatic water $\delta^{18}O$ = 8.0 ‰	6.2	320	Magmatic water $\delta^{18}O$ = 7.5 ‰	6.7	320	Magmatic water $\delta^{18}O$ = 7.7 ‰	6.4	285
		Avg.	**12.49**		**4.5**	**380**		**5.0**	**380**		**4.8**	**355**
		Min.	10.75		2.9	460		3.4	465		3.2	465
Late medium gray-CL quartz	450	Max.	12.61		4.5	380		5.2	375		4.9	350
		Avg.	**11.17**		**3.1**	**450**		**3.6**	**450**		**3.5**	**440**
		Min.	9.71		1.7	540		2.2	545		2.0	585
Requilibrated EDM	500	Max.	11.10		3.2	445		3.6	450		3.4	445
		Avg.	**10.66**		**2.7**	**475**		**3.2**	**475**		**2.9**	**485**
		Min.	10.23		2.2	505		2.8	505		2.5	525
Requilibrated B vein	550	Max.	11.39		3.4	430		3.9	435		3.7	425
		Avg.	**10.58**		**2.7**	**475**		**3.1**	**480**		**2.9**	**490**
		Min.	9.77		1.7	540		2.3	540		2.1	580

Note: T (°C) [preferred minimum estimate] taken from Table A5. * Experimental range for each fractionation calibration. Min. = Minimum, Avg. = Average, Max. = Maximum. Minimum and maximum represent the range of the average ± 2 standard deviations. Different magmatic water compositions are assumed in order to fix the calculated temperature of the dark gray-CL quartz at ~450 °C and the dark-CL quartz at ~340 to 380 °C using different fractionation factors. The dark-CL and dark gray-CL temperatures are reproduced well in all the calculations. EDM and B vein quartz show almost identical oxygen isotope compositions that always yield equal and lower than expected temperatures. For the discussion we assume a magmatic water composition of δ18O = 7.5 ‰ (Taylor, 1986) and fractionation factors from Zhang et al., 1989 since the experimental temperature range overlaps with the porphyry hydrothermal temperature range. However, the temperature estimates using the other fractionation factors show minimal variation.

Introduction to Table DR8: Known fractionation factors for $\delta^{18}O$ of quartz-water were used to estimate the range of permissive $\delta^{18}O$ of the magmatic water. Depending on the fractionation factor used, the possible values for water range from ~7.5 to 8.0 ‰ to yield the observed $\delta^{18}O$ of quartz at temperatures that are estimated independently from TitaniQ, fluid inclusion data and phase petrology. Note that since the EDM and B vein quartz appears to have partially re-equilibrated at ~ 450 ºC, the calculations of magmatic water composition are based on the ~450 ºC and ~350 ºC D vein quartz.

We assume that a single composition of magmatic-hydrothermal fluid produced all veins from high to low temperature (BQ to D veins), as proposed by Reed *et al.* (2013). It is not possible to assess whether the $\delta^{18}O$ of the magmatic water changes from one fluid input to another. However, this seems unlikely given that the composition of the intrusions in porphyry copper deposits is relatively fixed. Where the roots of other large porphyry copper deposits can be observed (*e.g.* Yerington, Dilles, 1987), they are underlain by a source granite that has uniform composition. The intrusions range from tonalite to granite, but at Haquira East are presumed to be granodiorite as this is the composition of the Haquira stock and the porphyry dikes. It is also not possible to assess whether the $\delta^{18}O$ of the water is significantly modified from the magmatic value by water-rock exchange between ~700 °C magmatic temperatures and the ~450 °C temperatures at which we calculate the quartz-water fractionation factor and water composition. However, it is unlikely that the magmatic water changed significantly on the basis that the quartz vein volume is very high (3 to >10 vol. %) and therefore the water : rock ratio was also high. Quartz solubility changes suggest that ~1000 ppm quartz would be precipitated during cooling, so this would require ~1000:1 water mass to vein quartz mass precipitated (Fournier, 1985). Furthermore, the water is ascending from the magma quickly by hydro-fracturing the wall-rock and therefore quickly depressurizing and cooling along a path that is close to adiabatic. Therefore, it is unlikely that at >350°C there is any meteoric water that mixes with the magmatic fluid (*cf.* Weis *et al.,* 2012)

Table DR9. RAW $\delta^{18}O$ IN QUARTZ SIMS DATA

Name Box

File	Comment	$\delta^{18}O$ ‰ VSMOW	2SD (ext.)	Mass Bias (‰)	$\delta^{18}O$ ‰ measured	2SE (int.)	^{16}O (Gcps)	IP (nA)	Yield (Gcps/nA)	Date	Time	X	Y	DTFA-X	DTFA-Y	$^{16}OH/^{16}O$	
SAMPLE:	**FC-HAQ-009**																
~~20150203@31.asc~~	~~009 UWQ-1 g0~~				~~5.963~~	~~0.234~~	~~2.833~~	~~**1.828**~~	~~1.550~~	~~2/3/15~~	~~8:45~~	~~-485~~	~~138~~	~~-8~~	~~-13~~	~~6.805E-05~~	discarded
20150203@32.asc	009 UWQ-1 g0				5.456	0.238	2.892	**1.829**	1.581	2/3/15	8:49	-412	-57	-9	-16	6.680E-05	
20150203@33.asc	009 UWQ-1 g1				5.585	0.273	2.849	**1.821**	1.564	2/3/15	8:53	1066	1462	-12	-15	6.453E-05	
20150203@34.asc	009 UWQ-1 g1				5.669	0.319	2.805	**1.810**	1.550	2/3/15	8:56	1243	1322	-12	-15	6.215E-05	
20150203@35.asc	009 UWQ-1 g0				5.872	0.230	2.836	**1.805**	1.572	2/3/15	9:00	-425	-20	-9	-17	7.126E-05	
	average and 2SD				**5.646**	**0.349**											
20150203@36.asc	009 D-vein	**9.71**	**0.32**		3.072	0.301	2.784	**1.800**	1.547	2/3/15	9:06	430	-2199	-2	-25	7.710E-05	
20150203@37.asc	009 D-vein	**13.62**	**0.32**		6.952	0.414	2.755	**1.794**	1.536	2/3/15	9:10	447	-2111	-2	-27	6.281E-05	
20150203@38.asc	009 D-vein	**10.78**	**0.32**		4.131	0.493	2.740	**1.788**	1.533	2/3/15	9:13	474	-2060	-1	-26	8.297E-05	
20150203@39.asc	009 D-vein	**13.60**	**0.32**		6.937	0.216	2.709	**1.779**	1.522	2/3/15	9:17	567	-2035	-5	-25	6.201E-05	
20150203@40.asc	009 D-vein	**10.60**	**0.32**		3.950	0.532	2.739	**1.773**	1.545	2/3/15	9:21	614	-2070	-4	-25	9.359E-05	
20150203@41.asc	009 D-vein	**11.49**	**0.32**		4.832	0.215	2.754	**1.764**	1.562	2/3/15	9:25	437	-1830	-4	-24	1.651E-04	
20150203@42.asc	009 D-vein	**11.13**	**0.32**		4.481	0.334	2.755	**1.756**	1.569	2/3/15	9:29	411	-1889	-3	-24	5.760E-05	
20150203@43.asc	009 D-vein	**11.38**	**0.32**		4.723	0.234	2.716	**1.748**	1.554	2/3/15	9:33	345	-1947	-2	-25	5.491E-05	
20150203@44.asc	009 D-vein	**10.89**	**0.32**		4.238	0.297	2.716	**1.738**	1.563	2/3/15	9:37	209	-2105	0	-26	5.232E-05	
20150203@45.asc	009 D-vein	**11.02**	**0.32**		4.371	0.328	2.677	**1.729**	1.548	2/3/15	9:40	165	-2193	1	-27	5.229E-05	
20150203@46.asc	009 UWQ-1 g0				5.637	0.188	2.675	**1.713**	1.562	2/3/15	9:44	-464	-200	-8	-19	5.278E-05	
~~20150203@47.asc~~	~~009 UWQ-1 g0~~				~~5.208~~	~~0.352~~	~~2.637~~	~~**1.704**~~	~~1.548~~	~~2/3/15~~	~~9:48~~	~~-467~~	~~-275~~	~~-7~~	~~-21~~	~~5.325E-05~~	discarded
20150203@48.asc	009 UWQ-1 g0 Cs-Res=118				5.904	0.266	2.736	**1.752**	1.561	2/3/15	9:53	-525	-144	-7	-20	4.923E-05	
20150203@49.asc	009 UWQ-1 g0				5.733	0.268	2.742	**1.760**	1.558	2/3/15	9:57	-546	-234	-6	-21	5.064E-05	
20150203@50.asc	009 UWQ-1 g0				5.514	0.218	2.772	**1.761**	1.574	2/3/15	10:00	-456	-131	-8	-19	4.898E-05	
	average and 2SD				**5.697**	**0.329**											
	bracket average and 2SD	**12.33**		**-6.58**	**5.671**	**0.319**											
SAMPLE:	**FC-HAQ-048**																
20150203@51.asc	048 UWQ-1 g0				5.819	0.251	2.782	**1.746**	1.594	2/3/15	10:09	166	-538	3	12	3.998E-05	
20150203@52.asc	048 UWQ-1 g0				5.582	0.241	2.801	**1.743**	1.607	2/3/15	10:13	248	-520	1	13	4.106E-05	
20150203@53.asc	048 UWQ-1 g1				5.742	0.241	2.790	**1.744**	1.599	2/3/15	10:16	297	1182	0	6	4.301E-05	
20150203@54.asc	048 UWQ-1 g1				5.604	0.353	2.790	**1.740**	1.603	2/3/15	10:20	323	1071	0	6	4.292E-05	
	average and 2SD				**5.687**	**0.226**											

File	Comment	$\delta^{18}O$ ‰ VSMOW	2SD (ext.)	Mass Bias (‰)	$\delta^{18}O$ ‰ measured	2SE (int.)	^{16}O (Gcps)	IP (nA)	Yield (Gcps/nA)	Date	Time	X	Y	DTFA-X	DTFA-Y	$^{16}OH/^{16}O$
20150203@55.asc	048 Late dark CL quartz	**12.75**	**0.22**		6.178	0.230	2.687	**1.737**	1.546	2/3/15	10:26	-1565	1716	-8	5	4.167E-05
20150203@56.asc	048 Late dark CL quartz	**12.57**	**0.22**		5.993	0.331	2.737	**1.733**	1.580	2/3/15	10:31	-1590	1736	-8	7	4.403E-05
20150203@57.asc	048 Late dark CL quartz	**12.76**	**0.22**		6.184	0.227	2.728	**1.727**	1.580	2/3/15	10:34	-1610	1749	-7	8	4.270E-05
20150203@58.asc	048 Late dark CL quartz	**13.07**	**0.22**		6.490	0.246	2.724	**1.721**	1.583	2/3/15	10:38	-1643	1752	-8	9	4.179E-05
20150203@59.asc	048 Late dark CL quartz	**12.52**	**0.22**		5.944	0.261	2.710	**1.714**	1.581	2/3/15	10:42	-1657	1769	-8	8	4.064E-05
20150203@60.asc	048 Late dark CL quartz	**11.57**	**0.22**		5.002	0.236	2.703	**1.707**	1.584	2/3/15	10:46	-1660	1795	-8	8	4.030E-05
20150203@61.asc	048 B vein	**10.54**	**0.22**		3.981	0.267	2.702	**1.700**	1.589	2/3/15	10:50	-1687	1803	-9	9	4.318E-05
20150203@62.asc	048 B vein	**10.61**	**0.22**		4.046	0.259	2.692	**1.694**	1.589	2/3/15	10:54	-1715	1813	-8	8	4.164E-05
20150203@63.asc	048 B vein	**10.35**	**0.22**		3.794	0.232	2.686	**1.690**	1.590	2/3/15	10:58	-1749	1823	-8	8	4.081E-05
20150203@64.asc	048 B vein	**10.24**	**0.22**		3.685	0.329	2.686	**1.687**	1.593	2/3/15	11:02	-1784	1839	-8	8	4.043E-05
20150203@65.asc	048 B vein	**10.51**	**0.22**		3.954	0.256	2.662	**1.683**	1.582	2/3/15	11:06	-1811	1849	-8	7	4.172E-05
20150203@66.asc	048 B vein	**10.36**	**0.22**		3.801	0.295	2.670	**1.681**	1.588	2/3/15	11:10	-1840	1861	-7	8	4.117E-05
20150203@67.asc	048 B vein	**10.10**	**0.22**		3.544	0.276	2.677	**1.679**	1.594	2/3/15	11:14	-1869	1880	-7	8	4.444E-05
20150203@68.asc	048 B vein	**10.34**	**0.22**		3.784	0.251	2.669	**1.676**	1.593	2/3/15	11:17	-1897	1895	-7	7	4.850E-05
20150203@69.asc	048 B vein	**10.29**	**0.22**		3.733	0.303	2.662	**1.673**	1.592	2/3/15	11:21	-1925	1910	-6	8	4.148E-05
20150203@70.asc	048 UWQ-1 g0				5.794	0.326	2.648	**1.661**	1.594	2/3/15	11:25	299	-565	-2	13	3.973E-05
20150203@71.asc	048 UWQ-1 g0				5.881	0.290	2.654	**1.658**	1.601	2/3/15	11:29	307	-600	-2	12	4.039E-05
20150203@72.asc	048 UWQ-1 g0				5.798	0.262	2.640	**1.656**	1.595	2/3/15	11:32	324	-644	-3	11	4.029E-05
20150203@73.asc	048 UWQ-1 g0				5.847	0.283	2.636	**1.653**	1.595	2/3/15	11:36	343	-685	-2	11	4.008E-05
	average and 2SD				**5.830**	**0.083**										
	bracket average and 2SD	**12.33**		**-6.49**	**5.758**	**0.220**										
20150203@74.asc	048 B vein	**10.42**	**0.27**		3.946	0.251	2.623	**1.651**	1.589	2/3/15	11:41	-1950	1922	-7	7	4.447E-05
20150203@75.asc	048 B vein	**10.47**	**0.27**		3.995	0.161	2.612	**1.647**	1.586	2/3/15	11:45	-1979	1938	-8	7	4.533E-05
20150203@76.asc	048 B vein	**10.31**	**0.27**		3.837	0.245	2.606	**1.642**	1.587	2/3/15	11:49	-2017	1960	-7	7	4.000E-05
20150203@77.asc	048 Late dark CL quartz	**12.40**	**0.27**		5.906	0.236	2.587	**1.635**	1.582	2/3/15	11:53	-1570	1752	-8	8	4.952E-05
20150203@78.asc	048 Late dark CL quartz	**12.71**	**0.27**		6.214	0.256	2.565	**1.629**	1.574	2/3/15	11:57	-1587	1772	-8	9	4.454E-05
20150203@79.asc	048 Late dark CL quartz	**12.96**	**0.27**		6.466	0.239	2.566	**1.624**	1.579	2/3/15	12:00	-1610	1792	-9	8	4.029E-05
20150203@80.asc	048 Late dark CL quartz	**11.71**	**0.27**		5.223	0.214	2.561	**1.620**	1.582	2/3/15	12:04	-1629	1809	-10	8	3.910E-05
20150203@81.asc	048 B vein	**10.76**	**0.27**		4.281	0.204	2.571	**1.617**	1.589	2/3/15	12:08	-1653	1828	-10	8	4.051E-05
20150203@82.asc	048 B vein	**10.90**	**0.27**		4.420	0.267	2.551	**1.614**	1.580	2/3/15	12:12	-1674	1824	-10	8	4.841E-05
20150203@83.asc	048 B vein	**10.52**	**0.27**		4.038	0.275	2.550	**1.611**	1.583	2/3/15	12:16	-1692	1831	-10	8	4.240E-05
20150203@84.asc	048 B vein	**10.60**	**0.27**		4.118	0.314	2.547	**1.607**	1.585	2/3/15	12:20	-1724	1842	-9	8	4.246E-05
20150203@85.asc	048 B vein	**10.08**	**0.27**		3.606	0.248	2.544	**1.604**	1.586	2/3/15	12:24	-1757	1854	-9	8	4.040E-05
20150203@86.asc	048 B vein	**10.21**	**0.27**		3.738	0.158	2.541	**1.601**	1.587	2/3/15	12:27	-1784	1864	-9	8	4.408E-05
20150203@87.asc	048 B vein	**10.20**	**0.27**		3.728	0.267	2.523	**1.599**	1.578	2/3/15	12:31	-1867	1907	-8	8	2.460E-04

File	Comment	$\delta^{18}O$ ‰ VSMOW	2SD (ext.)	Mass Bias (‰)	$\delta^{18}O$ ‰ measured	2SE (int.)	^{16}O (Gcps)	IP (nA)	Yield (Gcps/nA)	Date	Time	X	Y	DTFA-X	DTFA-Y	$^{16}OH/^{16}O$
20150203@88.asc	048 B vein	**10.09**	**0.27**		3.615	0.289	2.531	**1.597**	1.585	2/3/15	12:35	-1926	1938	-8	8	4.432E-05
20150203@89.asc	048 UWQ-1 g0				5.749	0.283	2.518	**1.584**	1.590	2/3/15	12:38	210	-518	1	12	3.702E-05
20150203@90.asc	048 UWQ-1 g0				5.684	0.314	2.519	**1.581**	1.594	2/3/15	12:42	136	-538	2	11	3.720E-05
20150203@91.asc	048 UWQ-1 g0 Cs-Res=119				6.144	0.245	2.584	**1.642**	1.574	2/3/15	12:48	148	-560	2	11	3.624E-05
20150203@92.asc	048 UWQ-1 g0				5.826	0.245	2.638	**1.649**	1.600	2/3/15	12:51	148	-505	2	12	3.699E-05
	average and 2SD				**5.851**	**0.408**										
	bracket average and 2SD	**12.33**		**-6.41**	**5.840**	**0.273**										
SAMPLE:	**FC-HAQ-027**															
20150203@93.asc	027 UWQ-1 g0				6.121	0.280	2.564	**1.651**	1.553	2/3/15	13:02	-907	*289*	12	-6	2.819E-05
20150203@94.asc	027 UWQ-1 g0				5.617	0.274	2.599	**1.651**	1.574	2/3/15	13:05	-1004	186	12	-7	2.926E-05
20150203@95.asc	027 UWQ-1 g1				5.738	0.211	2.594	**1.646**	1.575	2/3/15	13:09	486	-403	10	-8	2.893E-05
20150203@96.asc	027 UWQ-1 g1				5.569	0.306	2.588	**1.648**	1.571	2/3/15	13:12	537	-544	9	-10	2.938E-05
20150203@97.asc	027 UWQ-1 g0				5.806	0.288	2.587	**1.645**	1.572	2/3/15	13:16	-983	164	-12	-7	2.962E-05
	average and 2SD				**5.683**	**0.218**										
20150203@98.asc	027 B vein	**10.91**	**0.20**		4.286	0.220	2.533	**1.643**	1.541	2/3/15	13:22	-1080	2045	7	9	2.959E-05
20150203@99.asc	027 B vein	**10.91**	**0.20**		4.281	0.223	2.564	**1.640**	1.563	2/3/15	13:28	-1082	2030	7	9	3.035E-05
20150203@100.asc	027 B vein	**10.63**	**0.20**		4.000	0.210	2.592	**1.636**	1.584	2/3/15	13:32	-1084	1980	6	7	3.080E-05
20150203@101.asc	027 B vein	**10.80**	**0.20**		4.172	0.328	2.595	**1.632**	1.590	2/3/15	13:36	-1084	1937	7	7	2.943E-05
20150203@102.asc	027 B vein	**10.66**	**0.20**		4.031	0.302	2.583	**1.627**	1.588	2/3/15	13:40	-1086	1887	7	6	2.908E-05
20150203@103.asc	027 B vein	**10.49**	**0.20**		3.863	0.245	2.587	**1.625**	1.591	2/3/15	13:44	-1082	1842	7	4	3.319E-05
20150203@104.asc	027 B vein	**10.61**	**0.20**		3.982	0.295	2.567	**1.623**	1.581	2/3/15	13:47	-1082	1794	7	3	2.992E-05
20150203@105.asc	027 B vein	**10.80**	**0.20**		4.170	0.207	2.569	**1.622**	1.584	2/3/15	13:51	-1080	1749	7	2	2.922E-05
20150203@106.asc	027 B vein	**10.65**	**0.20**		4.028	0.269	2.558	**1.621**	1.578	2/3/15	13:55	-1077	1706	6	1	3.235E-05
20150203@107.asc	027 B vein	**10.64**	**0.20**		4.013	0.251	2.575	**1.621**	1.588	2/3/15	13:58	-1075	1634	6	1	3.188E-05
20150203@108.asc	027 B vein	**10.72**	**0.20**		4.095	0.255	2.554	**1.619**	1.577	2/3/15	14:02	-1070	1576	7	0	2.900E-05
20150203@109.asc	027 EDM	**10.96**	**0.20**		4.332	0.266	2.599	**1.617**	1.607	2/3/15	14:06	-1071	1519	7	-1	1.158E-04
20150203@110.asc	027 EDM	**10.63**	**0.20**		4.000	0.310	2.543	**1.614**	1.576	2/3/15	14:09	-1070	1476	7	-1	2.906E-05
20150203@111.asc	027 EDM	**10.73**	**0.20**		4.106	0.204	2.538	**1.610**	1.576	2/3/15	14:13	-1070	1404	7	-2	2.911E-05
20150203@112.asc	027 EDM	**10.76**	**0.20**		4.135	0.214	2.531	**1.607**	1.575	2/3/15	14:17	-1030	1315	7	-4	2.880E-05

File	Comment	$\delta^{18}O$ ‰ VSMOW	2SD (ext.)	Mass Bias (‰)	$\delta^{18}O$ ‰ measured	2SE (int.)	^{16}O (Gcps)	IP (nA)	Yield (Gcps/nA)	Date	Time	X	Y	DTFA-X	DTFA-Y	$^{16}OH/^{16}O$
20150203@113.asc	027 UWQ-1 g0				5.764	0.354	2.517	**1.603**	1.570	2/3/15	14:21	-795	267	6	-8	2.870E-05
20150203@114.asc	027 UWQ-1 g0				5.824	0.221	2.514	**1.602**	1.570	2/3/15	14:25	-847	300	6	-8	2.875E-05
20150203@115.asc	027 UWQ-1 g0 Cs-Res=120				5.613	0.243	2.620	**1.660**	1.578	2/3/15	14:31	-974	311	7	-6	2.569E-05
20150203@116.asc	027 UWQ-1 g0				5.608	0.233	2.649	**1.671**	1.585	2/3/15	14:35	-1038	307	8	-6	2.707E-05
	average and 2SD				**5.702**	**0.218**										
	bracket average and 2SD	**12.33**		**-6.56**	**5.692**	**0.203**										
20150203@117.asc	027 EDM	**12.39**	**0.20**		5.807	0.186	2.663	**1.680**	1.585	2/3/15	14:39	-1067	1224	7	-5	5.659E-05
20150203@118.asc	027 EDM	**10.62**	**0.20**		4.044	0.214	2.657	**1.680**	1.582	2/3/15	14:43	-1050	1201	7	-5	3.215E-05
20150203@119.asc	027 EDM	**10.11**	**0.20**		3.541	0.246	2.733	**1.679**	1.628	2/3/15	14:47	-1053	1146	7	-6	3.413E-05
20150203@120.asc	027 EDM	**11.32**	**0.20**		4.747	0.371	2.691	**1.676**	1.606	2/3/15	14:50	-1047	1084	8	-6	1.337E-04
20150203@121.asc	027 EDM	**10.64**	**0.20**		4.072	0.251	2.628	**1.672**	1.571	2/3/15	14:54	-1044	974	8	-8	2.771E-05
20150203@122.asc	027 EDM	**10.74**	**0.20**		4.165	0.282	2.604	**1.667**	1.562	2/3/15	14:58	-1044	902	8	-9	2.757E-05
20150203@123.asc	027 EDM	**10.78**	**0.20**		4.202	0.299	2.535	**1.665**	1.523	2/3/15	15:02	-1038	820	8	-12	2.906E-05
20150203@124.asc	027 B vein	**10.59**	**0.20**		4.014	0.215	2.604	**1.667**	1.563	2/3/15	15:06	-345	2130	4	7	2.314E-05
20150203@125.asc	027 B vein	**10.49**	**0.20**		3.915	0.246	2.624	**1.662**	1.578	2/3/15	15:10	-346	2100	2	6	4.955E-05
20150203@126.asc	027 B vein	**10.39**	**0.20**		3.823	0.252	2.623	**1.654**	1.585	2/3/15	15:15	-311	2060	3	6	3.850E-05
20150203@127.asc	027 B vein	**10.44**	**0.20**		3.864	0.240	2.621	**1.647**	1.592	2/3/15	15:19	-319	2023	3	7	2.697E-05
20150203@128.asc	027 B vein	**10.48**	**0.20**		3.905	0.227	2.628	**1.644**	1.599	2/3/15	15:22	-324	2003	3	7	2.858E-05
20150203@129.asc	027 B vein	**10.36**	**0.20**		3.786	0.201	2.625	**1.646**	1.595	2/3/15	15:26	-215	2018	2	6	2.734E-05
20150203@130.asc	027 B vein	**10.84**	**0.20**		4.265	0.327	2.580	**1.645**	1.568	2/3/15	15:31	-277	989	5	-5	2.831E-05
20150203@131.asc	027 B vein	**10.85**	**0.20**		4.280	0.309	2.551	**1.643**	1.553	2/3/15	15:35	-365	825	6	-7	1.006E-03
20150203@132.asc	027 UWQ-1 g1				5.733	0.246	2.590	**1.629**	1.590	2/3/15	15:40	401	-301	10	-7	2.590E-05
20150203@133.asc	027 UWQ-1 g1				5.701	0.300	2.560	**1.630**	1.571	2/3/15	15:43	447	-353	9	-8	3.396E-05
20150203@134.asc	027 UWQ-1 g1				5.864	0.270	2.560	**1.630**	1.570	2/3/15	15:47	445	-452	9	-9	2.566E-05
20150203@135.asc	027 UWQ-1 g1				5.865	0.282	2.564	**1.629**	1.574	2/3/15	15:50	598	-465	7	-10	2.604E-05
	average and 2SD				**5.791**	**0.172**										
	bracket average and 2SD	**12.33**		**-6.50**	**5.747**	**0.205**										
20150203@136.asc	009 UWQ-1 g0				5.872	0.301	2.527	**1.619**	1.560	2/3/15	15:59	-496	-183	-8	-14	2.853E-05
20150203@137.asc	009 UWQ-1 g0				5.878	0.273	2.524	**1.618**	1.560	2/3/15	16:02	-540	-198	-6	-15	2.909E-05
20150203@138.asc	009 UWQ-1 g0				6.040	0.211	2.533	**1.617**	1.567	2/3/15	16:06	-566	-138	-5	-15	2.979E-05
20150203@139.asc	009 UWQ-1 g0				5.770	0.239	2.530	**1.614**	1.568	2/3/15	16:10	-561	-83	-6	-14	2.959E-05

File	Comment	$\delta^{18}O$ ‰ VSMOW	2SD (ext.)	Mass Bias (‰)	$\delta^{18}O$ ‰ measured	2SE (int.)	^{16}O (Gcps)	IP (nA)	Yield (Gcps/nA)	Date	Time	X	Y	DTFA-X	DTFA-Y	$^{16}OH/^{16}O$
SAMPLE:	**FC-HAQ-009**															
20150203@140.asc	009 D-vein	**13.34**	**0.22**		6.889	0.271	2.493	**1.616**	1.542	2/3/15	16:15	477	-1795	-4	-19	1.249E-04
20150203@141.asc	009 D-vein	**12.53**	**0.22**		6.081	0.291	2.521	**1.613**	1.563	2/3/15	16:19	501	-1773	-5	-18	1.389E-04
20150203@142.asc	009 D-vein	**13.01**	**0.22**		6.560	0.261	2.509	**1.610**	1.559	2/3/15	16:23	537	-1761	-5	-18	3.625E-05
20150203@143.asc	009 D-vein	**12.93**	**0.22**		6.481	0.249	2.496	**1.608**	1.552	2/3/15	16:26	562	-1740	-5	-18	3.530E-05
20150203@144.asc	009 D-vein	**13.10**	**0.22**		6.651	0.354	2.483	**1.605**	1.547	2/3/15	16:30	598	-1713	-6	-18	6.744E-04
20150203@145.asc	009 D-vein	**11.39**	**0.22**		4.951	0.382	2.493	**1.603**	1.556	2/3/15	16:33	628	-1680	-6	-17	3.317E-05
20150203@146.asc	009 UWQ-1 g0				5.858	0.308	2.480	**1.592**	1.557	2/3/15	16:38	-507	-219	-6	-15	3.080E-05
20150203@147.asc	009 UWQ-1 g0				5.720	0.282	2.482	**1.591**	1.560	2/3/15	16:41	-584	-171	-5	-15	3.020E-05
20150203@148.asc	009 UWQ-1 g0 Cs-Res=121				6.014	0.295	2.564	**1.654**	1.550	2/3/15	16:48	-602	-148	-5	-15	3.011E-05
20150203@149.asc	009 UWQ-1 g0				5.898	0.269	2.590	**1.663**	1.557	2/3/15	16:51	-646	-130	-4	-15	3.077E-05
	average and 2SD				**5.873**	**0.243**										
	bracket average and 2SD	**12.33**		**-6.37**	**5.881**	**0.217**										
20150203@150.asc	009 D-vein	**13.15**	**0.25**		6.648	0.261	2.583	**1.673**	1.544	2/3/15	16:56	663	-1647	-7	-16	3.363E-04
20150203@151.asc	009 D-vein	**11.18**	**0.25**		4.700	0.237	2.637	**1.674**	1.575	2/3/15	17:00	692	-1617	-7	-16	2.822E-05
20150203@152.asc	009 D-vein	**11.19**	**0.25**		4.707	0.248	2.612	**1.674**	1.560	2/3/15	17:04	744	-1589	-8	-16	5.766E-05
20150203@153.asc	009 D-vein	**11.09**	**0.25**		4.605	0.287	2.625	**1.672**	1.570	2/3/15	17:07	782	-1559	-7	-15	3.380E-05
20150203@154.asc	009 D-vein	**11.13**	**0.25**		4.646	0.225	2.632	**1.671**	1.575	2/3/15	17:11	825	-1532	-8	-15	6.250E-05
20150203@155.asc	009 D-vein	**10.69**	**0.25**		4.211	0.275	2.683	**1.670**	1.606	2/3/15	17:14	870	-1508	-8	-14	1.097E-04
20150203@156.asc	009 D-vein	**12.98**	**0.25**		6.482	0.263	2.571	**1.665**	1.545	2/3/15	17:19	230	-1804	-2	-19	3.252E-05
20150203@157.asc	009 D-vein	**13.15**	**0.25**		6.651	0.226	2.576	**1.662**	1.549	2/3/15	17:23	255	-1768	-2	-19	4.722E-05
20150203@158.asc	009 D-vein	**13.02**	**0.25**		6.527	0.233	2.583	**1.660**	1.556	2/3/15	17:27	279	-1725	-2	-19	3.412E-05
20150203@159.asc	009 D-vein	**13.14**	**0.25**		6.643	0.240	2.578	**1.659**	1.554	2/3/15	17:30	304	-1683	-3	-18	3.440E-05
20150203@160.asc	009 D-vein	**11.91**	**0.25**		5.417	0.252	2.593	**1.657**	1.564	2/3/15	17:34	318	-1643	-4	-18	5.878E-05
20150203@161.asc	009 D-vein	**12.02**	**0.25**		5.530	0.343	2.594	**1.657**	1.566	2/3/15	17:37	340	-1614	-4	-18	8.513E-05
20150203@162.asc	009 D-vein	**11.43**	**0.25**		4.941	0.295	2.581	**1.655**	1.560	2/3/15	17:41	354	-1573	-4	-18	3.033E-05
20150203@163.asc	009 D-vein	**12.41**	**0.25**		5.921	0.214	2.574	**1.651**	1.559	2/3/15	17:45	368	-1527	-5	-17	3.305E-05
20150203@164.asc	009 D-vein	**10.84**	**0.25**		4.358	0.300	2.688	**1.646**	1.633	2/3/15	17:49	384	-1484	-5	-17	3.872E-05
20150203@165.asc	009 UWQ-1 g0				5.917	0.276	2.539	**1.631**	1.557	2/3/15	17:54	-505	-265	-15	-15	2.857E-05
20150203@166.asc	009 UWQ-1 g0				5.829	0.306	2.555	**1.628**	1.570	2/3/15	17:58	-443	-240	-16	-14	2.833E-05
20150203@167.asc	009 UWQ-1 g0				5.851	0.285	2.553	**1.625**	1.571	2/3/15	18:01	-493	-114	-16	-13	2.899E-05

File	Comment	$\delta^{18}O$ ‰ VSMOW	2SD (ext.)	Mass Bias (‰)	$\delta^{18}O$ ‰ measured	2SE (int.)	^{16}O (Gcps)	IP (nA)	Yield (Gcps/nA)	Date	Time	X	Y	DTFA-X	DTFA-Y	$^{16}OH/^{16}O$
20150203@168.asc	009 UWQ-1 g0				5.615	0.215	2.556	**1.625**	1.573	2/3/15	18:05	-415	-122	-17	-12	2.858E-05
	average and 2SD				**5.803**	**0.262**										
	bracket average and 2SD	**12.33**		**-6.41**	**5.838**	**0.245**										
SAMPLE:	**FC-HAQ-004**							**Cs-Res=122**								
20150203@169.asc	004 UWQ-1 g0				5.851	0.278	2.666	**1.683**	1.584	2/3/15	18:16	-1393	-389	2	5	2.602E-05
20150203@170.asc	004 UWQ-1 g0				5.691	0.204	2.702	**1.691**	1.598	2/3/15	18:19	-1406	-332	3	6	2.644E-05
20150203@171.asc	004 UWQ-1 g0				5.655	0.270	2.718	**1.692**	1.606	2/3/15	18:23	-1355	-359	3	5	2.813E-05
20150203@172.asc	004 UWQ-1 g0				5.566	0.221	2.713	**1.696**	1.600	2/3/15	18:26	-1326	-409	2	3	2.738E-05
	average and 2SD				**5.691**	**0.238**										
20150203@173.asc	004 Late dark CL quartz	**13.14**	**0.22**		6.453	0.264	2.715	**1.703**	1.594	2/3/15	18:31	1734	-660	-1	-3	2.686E-05
20150203@174.asc	004 B vein	**10.66**	**0.22**		3.990	0.268	2.698	**1.702**	1.585	2/3/15	18:35	1692	-627	-2	-3	3.773E-05
20150203@175.asc	004 B vein	**10.46**	**0.22**		3.794	0.263	2.699	**1.700**	1.588	2/3/15	18:38	1648	-577	-2	-2	3.181E-05
20150203@176.asc	004 B vein	**10.43**	**0.22**		3.765	0.238	2.703	**1.699**	1.591	2/3/15	18:42	1614	-550	-2	-2	3.023E-05
20150203@177.asc	004 B vein	**10.61**	**0.22**		3.939	0.236	2.688	**1.698**	1.583	2/3/15	18:46	1555	-507	-1	-2	3.852E-05
20150203@178.asc	004 B vein	**10.51**	**0.22**		3.840	0.283	2.685	**1.695**	1.584	2/3/15	18:49	1388	-421	0	-2	3.072E-05
20150203@179.asc	004 B vein	**12.88**	**0.22**		6.199	0.266	2.669	**1.696**	1.574	2/3/15	18:53	1732	-694	-2	-3	4.054E-05
20150203@180.asc	004 B vein	**10.79**	**0.22**		4.117	0.282	2.674	**1.694**	1.579	2/3/15	18:57	1708	-672	-2	-3	3.411E-05
20150203@181.asc	004 B vein	**10.62**	**0.22**		3.952	0.296	2.672	**1.692**	1.580	2/3/15	19:01	1691	-655	-1	-3	3.183E-05
20150203@182.asc	004 Late dark CL quartz	**13.08**	**0.22**		6.396	0.265	2.660	**1.690**	1.574	2/3/15	19:04	1757	-660	-1	-3	2.826E-05
20150203@183.asc	004 Late dark CL quartz	**11.28**	**0.22**		4.612	0.186	2.650	**1.685**	1.573	2/3/15	19:09	1802	-749	-2	-2	2.611E-05
20150203@184.asc	004 Late dark CL quartz	**11.05**	**0.22**		4.383	0.262	2.655	**1.682**	1.579	2/3/15	19:13	1938	-889	-2	-4	2.821E-05
20150203@185.asc	004 B vein	**10.74**	**0.22**		4.074	0.301	2.670	**1.678**	1.591	2/3/15	19:16	2063	-1125	-3	-6	3.168E-05
20150203@186.asc	004 UWQ-1 g0				5.726	0.226	2.639	**1.673**	1.577	2/3/15	19:21	-1395	-280	6	6	2.713E-05
20150203@187.asc	004 UWQ-1 g0				5.645	0.191	2.699	**1.679**	1.608	2/3/15	19:25	-1364	-320	8	6	2.849E-05
20150203@188.asc	004 UWQ-1 g0				5.588	0.236	2.668	**1.675**	1.593	2/3/15	19:28	-1372	-425	7	2	2.799E-05
20150203@189.asc	004 UWQ-1 g0				5.482	0.238	2.669	**1.667**	1.601	2/3/15	19:32	-1418	-424	7	2	2.762E-05
	average and 2SD				**5.610**	**0.205**										
	bracket average and 2SD	**12.33**		**-6.60**	**5.651**	**0.223**										

Note: IP values in the table are 110pA lower than acutal PA

References

Antares, 2010, Antares press-release: New Haquira global resource. February 26th, 2010. 6 p.

Audétat, A., Garbe-Schönberg, D., Kronz, A., Pettke, T., Rusk, B., Donovan, J. J. and Lowers, H. A., 2014, Characterisation of a Natural Quartz Crystal as a Reference Material for Microanalytical Determination of Ti, Al, Li, Fe, Mn, Ga and Ge: Geostandards and Geoanalytical Research, v. 39, no. 2, p. 171-184.

Borradaile, G., 2003. Statistics of Earth Science Data. Their distribution in time, space and orientation. Springer, 352 pp.

Brimhall, G.H, Dilles, J.H., and Proffett, J.M., Jr., 2006, The role of geologic mapping in mineral exploration, in Doggett, M. D., and Parry, J. R., eds., Wealth creation in the minerals industry: Integrating, science, business, and education: Society of Economic Geologists Special Publication 12, p. 221-241.

Brimhall, G.H, Jr., 1977, Early fracture-controlled disseminated mineralization at Butte, Montana: Economic Geology, v. 72, p. 37-59.

Burnham, C.W., 1979, Magmas and hydrothermal fluids, *in* Barnes, H.L., ed., Geochemistry of hydrothermal ore deposits: New York, Wiley Interscience, v. II, p. 71-136.

Cernuschi, F., 2015, The geology and geochemistry of the Haquira East porphyry copper deposit of southern Peru: Insights on the timing, temperature and lifespan of the magmatic-hydrothermal alteration and mineralization: Unpub. PhD thesis, Oregon State University, 258 p.

Cernuschi, F., Dilles, J.H., and Creaser, R., 2013, Hydrothermal alteration, SWIR-mineral mapping, vein distribution and age of the Haquira-East Cu-Mo porphyry: 12th SGA Biennial Meeting 2013, Proceedings, v. 2, p. 782-785.

Cernuschi, F., Einaudi, M.T, Dilles, J.H., Heather, K.B., and Barr, N.C., 2012, Hydrothermal veins, porphyry geochemistry and mineralization zonation of the Haquira-East porphyry Cu-Mo deposit, Perú: SEG Conference 2012, Lima, Perú.

Chelle–Michou, C., 2013, Geochronologic and petrologic evolution of the magmatic suit associated with the Eocene Coroccohuayco deposit, and its role in the genesis of the associated Cu(-Au) porphyry-skarn mineralization, Tintaya District, Perú. Unpub. PhD thesis, University de Geneve, 254 pp.

Cherniak, D., Watson, E., and Wark, D., 2007, Ti diffusion in quartz: Chemical Geology, v. 236, p. 65–74, https://doi.org/10.1016/j.chemgeo.2006.09.001.

Clark, A.H., 1993, Are outsize porphyry copper deposits either anatomically or environmentally distinctive? : Society of Economic Geologists Special Publication 2, p. 213–282.

Cooke, DR, Hollings, P and Walshe, JL 2005 , 'Giant Porphyry Deposits: Characteristics, Distribution, and Tectonic Controls' , Economic Geology, vol. 100, no. 5 , pp. 801-818 ,

Crank, J., 1975, The mathematics of diffusion (2nd ed.). Oxford, Clarendon Press, 414 pp.

Dennis, P.F., 1984, Oxygen self-diffusion in quartz under hydrothermal conditions: Journal of Geophysical Research, v. 89, p. 4047–4057, https://doi.org/10.1029/JB089iB06p04047.

Dilles, J.H., 1987, Petrology of the Yerington batholith, Nevada: Evidence for evolution of porphyry copper ore fluids: Economic Geology, v. 82, p. 1750–1789.

Dilles, J.H., Tomlison, A.H., Garcia, M., and Alcota, H., 2011, The geology of the Fortuna Granodiorite Complex, Chuquicamata district, Northern Chile. Relation to porphyry copper deposits: 11th SGA Biennial Meeting 2011, Proceedings, v. 2, p. 398-400.

Dumitru, T.A., Ernst, W.G., Wright, J.E., Wooden, J.L., Wells, R.E., Farmer, L.P., Kent, A.J.R., Graham, S.A., 2013, Eocene extension in Idaho generated massive sediment floods into the Franciscan Trench and into the Tyee, Great Valley, and Green River Basins: Geology 41 (2), 187–190.

Ferry, J. M., Kitajima, K., Strickland, A and Valley, J. W., 2014, Ion microprobe survey of the grain-scale oxygen isotope geochemistry of minerals in metamorphic rocks: Geochimica et Cosmochimica Acta, v. 144, p. 403-433.

Field, C.W., Zhang, L., Dilles, J.H., Rye, R. O., and Reed, M.H., 2005, Sulfur and oxygen isotopic record in sulfate and sulfide minerals of early, deep, pre-main stage porphyry Cu-Mo and late main stage base-metal mineral deposits, Butte district, Montana: Chemical Geology, v. 215, no. 1-4, p. 61–93.

Fournier, R.O., 1985, The behavior of silica in hydrothermal solution: Reviews in Economic Geology, v. 2, p. 45-72.

Gans, P., 2009, Geology of the Haquira copper deposit: New information and synthesis: Internal report for Antares Minerals, 9 p.

Harris, A.C., and Golding, S.D., 2002, New evidence of magmatic-fluid-related phyllic alteration: Implications for the genesis of porphyry Cu deposits: Geology v. 30, p. 335–338.

Hu, G., & Clayton, R. N., 2003, Oxygen isotope salt effects at high pressure and high temperature and the calibration of oxygen isotope geothermometers. A Special Issue Dedicated to Robert Clayton, 67(17), 3227–3246.

Jochum, K. P., Weis, U., Stoll, B., Kuzmin, D., Yang, Q., Raczek, I., Jacob, D. E., Stracke, A., Birbaum, K., Frick, D. A., Günther, D. and Enzweiler, J., 2011, Determination of Reference Values for NIST SRM 610-617 Glasses Following ISO Guidelines: Geostandards and Geoanalytical Research, v. 35, no. 4, p. 397-429.

Kelly JL, Fu B, Kita NT, Valley JW (2007) Optically Continuous Silcrete Cements Of The St. Peter Sandstone: Oxygen Isotope Analysis By Ion Microprobe And Laser Fluorination. Geochem. Cosmochim. Acta. 71:3812-3832.

Kent, A.J.R., Jacobsen, B., Peate, D.W., Waight, T.E., and Baker, J.A., 2004, Isotope dilution MC-ICP-MS rare earth element analysis of geochemical reference materials NIST SRM 610, NIST SRM 612, NIST SRM 614, BHVO-2G, BHVO-2, BCR-2G, JB-2, WS-1, W-2, AGV-1, AGV-2. Geostandards Newsletter, 28(3), 417-430.

Kita, N.T., Ushikubo, T., Fu, B., Valley, J.W., 2009, High precision SIMS oxygen isotope analysis and the effect of sample topography: Chemical Geology, v. 264, p. 43–57.

Landtwing, M.R., Pettke, T., Halter, W.E., Heinrich, C.A., Redmond, P.B., Einaudi, M.T., and Kunze, K., 2005, Copper deposition during quartz dissolution by cooling hydrothermal fluids: The Bingham porphyry: Earth and Planetary Science Letters, v. 235, p. 229-243.

Loewen, M.W., and Kent, A.J., 2012, Sources of elemental fractionation and uncertainty during the analysis of semi-volatile metals in silicate glasses using LA-ICP-MS: Journal of Analytical and Atomic Spectrometry, v. 27, p. 1502-1508

Matsuhisa, Y., Goldsmith, J.R., and Clayton, R.N., 1979, Oxygen isotopic fractionation in the system quartz-albite-anorthite-water: Geochimica et Cosmochimica Acta, v. 43, no. 7, p. 1131–1140.

Mercer, C.N., and Reed, M.H., 2013, Porphyry Cu-Mo stockwork formation by dynamic, transient hydrothermal pulses: mineralogic insights from the deposit at Butte, Montana: Economic Geology, v. 108, no. 6, p. 1347–1377.

Nakashima D., Kita N. T., Ushikubo T., Noguchi T., Nakamura T. and Valley J. W. (2013) Oxygen three-isotope ratios of silicate particles returned from asteroid Itokawa by the Hay-abusa spacecraft: a strong link with equilibrated LL chondrites: Earth and Planetary Science Letters, v. 379, p. 127–136.

Proffett, J.M., 2009, High Cu grades in porphyry Cu deposits and their relationship to emplacement depth of magmatic sources: Geology, v. 37 (8), p. 675–678.

Reed, M., Rusk, B., and Palandri, J., 2013, The Butte magmatic-hydrothermal system: One fluid yields all alteration and veins: Economic Geology, v. 108, p. 1379–1396.

Rusk, B.G., Reed, M.H., and Dilles, J.H., 2008, Fluid inclusion evidence for magmatic-hydrothermal fluid evolution in the porphyry copper-molybdenum deposit at Butte, Montana: Economic Geology, v. 103, p. 307-334.

Rusk, B.G., Reed, M.H., Dilles, J.H., and Kent, A.J.R., 2006, Intensity of quartz cathodoluminescence and trace element content of quartz from the porphyry copper deposit in Butte, Montana: American Mineralogist, v. 91, p. 1300-1312.

Seedorff, E., Dilles, J.H., Proffett, J.M., Jr, Einaudi, M.T., Zurcher, L., Stavast, W.J.A., Johnson, D.A., Barton, M.D., 2005, Porphyry deposits: Characteristics and origin of hypogene features, *in* Hedenquist, J. W., Thompson, J. F. H., Goldfarb, R. J., and Richards, J. P., eds., Economic Geology 100th Anniversary Volume, p. 251-298.

Schöpa, A., Annen, C., Dilles, J. H., Sparks, R. S. J., and Blundy, J. D., 2017, Magma Emplacement Rates and Porphyry Copper Deposits: Thermal Modeling of the Yerington Batholith, Nevada. Economic Geology, 112(7), 1653-1672.

Stavast, W.J.A., Butler, B.F., Seedorff, E., Barton, M.D., and Ferguson, C.A., 2008, Tertiary tilting and dismemberment of the Laramide arc and related hydrothermal systems, Sierrita Mountains, Arizona: Economic Geology, v. 103, p. 629-636.

Taylor H.P., Jr., 1986, Igneous rocks: II. Isotopic case studies of circumpacific magmatism. Rev Mineral v. 16, p. 273-316.

Tenner T. J., Ushikubo T., Kurahashi E., Kita N. T. and Nagahara H. (2013) Oxygen isotope systematics of chondrule phenocrysts from the CO3.0 chondrite Yamato 82120: evidence for two distinct oxygen isotope reservoirs: Geochimica et Cosmochimica Acta, v. 102, p. 226–245.

Ushikubo T., Kimura M., Kita N. T. and Valley J. W. (2012) Primordial oxygen isotope reservoirs of the solar nebula recorded in chondrules in Acfer 094 carbonaceous chondrite: Geochimica et Cosmochimica Acta, v. 90, p. 242–264.

Valley, J. W., 2001, Stable isotope thermometry at high temperatures, in Reviews in Mineralogy and Geochemistry, v. 43, no. 1, p. 365–413.

Valley, J.W., Kita, N.T., 2009, In situ oxygen isotope geochemistry by ion microprobe, *in* Fayek, M. Ed., Secondary ion mass spectrometry in the earth sciences: Mineralogical Society of Canada Short Course, p. 19–63.

Von Quadt, A., Erni, M., Martinek, K., Moll, M., Peytcheva, I., and Heinrich, C.A., 2011, Zircon crystallization and the lifetimes of ore-forming magmatic-hydrothermal systems: Geology, v. 39, no. 8, p. 731–734.

Walker, B.A., Klemetti, E.W., Grunder, A.L., Dilles, J.H., Tepley, F.J., and Giles, D., 2013, Crystal reaming during the assembly, maturation, and waning of an eleven-million-year crustal magma cycle: thermobarometry of the Aucanquilcha Volcanic Cluster: Contributions to Mineralogy and Petrology, v. 165, no. 4, 663–682.

Watson, E. B., and Cherniak, D. J., 2015, Quantitative cooling histories from stranded diffusion profiles. Contributions to Mineralogy and Petrology, 169 (6).

Weis, P., Driesner, T. & Heinrich, C. A., 2012, Porphyry-copper ore shells form at stable pressure–temperature fronts within dynamic fluid plumes: Science, v. 338, p. 1613–1616.

Zhang L.-G., Liu J.-X., Zhou H.B. and Chen Z.-S., 1989, Oxygen isotope fractionation in the quartz-water-salt system. Economic Geology, 89, p. 1643-1650.